AFRL-AFOSR-VA-TR-2023-0395

Fully Passive and Ultra-Low-Power Technologies for Spectral Enhancement of Human Vision

Kats, Mikhail
UNIVERSITY OF WISCONSIN SYSTEM
21 N PARK ST STE 6301
MADISON, WI, 53715
USA

07/14/2023
Final Technical Report

Air Force Research Laboratory
Air Force Office of Scientific Research
Arlington, Virginia 22203
Air Force Materiel Command

REPORT DOCUMENTATION PAGE

PLEASE DO NOT RETURN YOUR FORM TO THE ABOVE ORGANIZATION.

1. REPORT DATE	2. REPORT TYPE	3. DATES COVERED	
20230714	Final	START DATE 20180301	END DATE 20220228

4. TITLE AND SUBTITLE
Fully Passive and Ultra-Low-Power Technologies for Spectral Enhancement of Human Vision

5a. CONTRACT NUMBER	5b. GRANT NUMBER	5c. PROGRAM ELEMENT NUMBER
	FA9550-18-1-0146	61102F
5d. PROJECT NUMBER	**5e. TASK NUMBER**	**5f. WORK UNIT NUMBER**

6. AUTHOR(S)
Mikhail Kats

7. PERFORMING ORGANIZATION NAME(S) AND ADDRESS(ES)
UNIVERSITY OF WISCONSIN SYSTEM
21 N PARK ST STE 6301
MADISON, WI 53715
USA

8. PERFORMING ORGANIZATION REPORT NUMBER

9. SPONSORING/MONITORING AGENCY NAME(S) AND ADDRESS(ES)	10. SPONSOR/MONITOR'S ACRONYM(S)	11. SPONSOR/MONITOR'S REPORT NUMBER(S)
Air Force Office of Scientific Research 875 N. Randolph St. Room 3112 Arlington, VA 22203	AFRL/AFOSR RTB1	AFRL-AFOSR-VA-TR-2023-0395

12. DISTRIBUTION/AVAILABILITY STATEMENT
A Distribution Unlimited: PB Public Release

13. SUPPLEMENTARY NOTES

14. ABSTRACT
In this YIP project, we achieved the following: 1. We identified an optical material—cesium lead bromide nanocrystals spun onto films and capped for protection—as an excellent candidate for fully passive down-conversion imaging. 2. We built and demonstrated an all-passive imaging system, demonstrating passive frequency conversion of ultraviolet images into the visible without any significant loss of imaging resolution. 3. We designed and demonstrated a fully passive device in the form factor of a pair of glasses that breaks binocular redundancy, with the goal of enhancing the wearer's ability to distinguished metameric spectra. 4. We demonstrated a new technique, hyperspectral interference tomography, which combines hyperspectral imaging with thin-film modeling to enable rapid nondestructive analysis of biominerals like nacre 5. We developed several metamaterial and metasurface
technologies to enable future developments in imaging and focusing, which can hopefully be
used in compact vision-enhanc ement systems. This includes metamaterials that must be described by more than one refractive index simultaneously, tunable metasurface componentsusing graphene nanoribbons, and inverse-design methods using coupled-mode theory to design very large-scale metasurfaces quickly. 6. We explored laser-light sails, demonstrating a design based on metasurfaces that self-stabilizes in a laser beam, and thus can "ride" the beam.

15. SUBJECT TERMS

16. SECURITY CLASSIFICATION OF:			17. LIMITATION OF ABSTRACT	18. NUMBER OF PAGES
a. REPORT U	b. ABSTRACT U	c. THIS PAGE U	UU	30

19a. NAME OF RESPONSIBLE PERSON	19b. PHONE NUMBER *(Include area code)*
GERNOT POMRENKE	426-8426

Standard Form 298 (Rev.5/2020)
Prescribed by ANSI Std. Z39.18

AFOSR Deliverable Reporting Format:
Final and Interim Reports

This document has been developed to provide Principal Investigators (PIs), co-PIs, and research organizations with:

- A listing of the questions that will be asked in the new AFOSR project reporting format;
- Assistance in planning for the submission of the report

Overview: There are two main sections of the AFOSR Deliverable Report. Section 1 is filled out in Qualtrics, and Section 2 is uploaded by PDF.

- Section 1: Structured Survey Questions in Qualtrics
  - This section captures information in a structured survey format as required by the Research Performance Progress Report Format (RPPR) guidance. Information in this section will include publications, participants, and other intellectual property questions. All questions in this section will be asked within Qualtrics.

- Section 2: Technical Report PDF
  - This section captures unstructured technical information not captured in the above section. PI's will upload PDF reports that contain information on awards, changes to scope, and other technical updates. This PDF upload will be very similar to previous AFOSR report uploads. Please contact your individual program officer if you have further questions about what should be contained in this report.

***Note: The information being asked in this deliverable report is explicitly defined by the official RPPR guidance which can be found here: http://www.nsf.gov/bfa/dias/policy/rppr/index.jsp. We have automated several questions to make the reporting less burdensome on the principal investigator. Your report link, found in the deliverable reminder email, contains individualized information that is specific to your deliverable report. You may edit this information if anything appears to be incorrect.

Section 2: Technical Report PDF Upload

You will be asked to complete the following questions as part of the report documentation section:

- Distribution Statement –Please verify that the report you are about to upload is cleared for public release through your organization's processes and procedures.
- Report Abstract
- Report Document - Upload the Report Document. File must be a PDF. Please do not password protect or secure the PDF. The maximum file size for the Report Document is 100MB.

Regarding the content of the report, we require the following sections in your PDF technical report upload.

Accomplishments

The information provided in this section allows AFOSR to assess whether satisfactory progress has been made during this reporting period. The PI is reminded that the recipient organization is required to obtain prior written approval from the awarding agency grants official whenever there are significant changes in the project or its direction. See agency specific instructions for submission of these requests.

- Research Objectives: Please list the main research objectives of this project
    - [From proposal] The design, fabrication, characterization, and implementation of a fully passive device in the form factor of a pair of glasses that breaks binocular redundancy in the spectral response, enhancing the wearer's ability to distinguish metameric spectra
    - [From proposal] Design and implementation of experimental setups to generate sets of metameric spectra on demand. The development of such setups is necessary for experimental verification of higher-dimensional vision, and for vision psychology experiments that will follow the present project
    - [From proposal] Evaluation and characterization of optical materials and devices for up- and down-conversion of photons into the visible range from the infrared and ultraviolet, respectively at conditions (*i.e.*, intensity, degree of coherence) relevant for vision enhancement.
    - [From proposal] Integration and testing of one or more spectrum-broadening materials and devices described in Objective 3 into an instrument that enables human vision beyond the visible spectral range.
    - [From proposal] Design of an optimal mapping strategy of ultraviolet and near-infrared bands into the visible to maximize the amount of simultaneous information presented to the user
    - [Added in consultation with PO] Development of hyperspectral imaging

technique to analyze biominerals
    - [Added in consultation with PO] Develop better understanding of the calculation of optical forces to enable laser light sails

- Please provide details of accomplishments during this reporting period.
    - We identified an optical material—cesium lead bromide nanocrystals spun onto films and capped for protection—as an excellent candidate for fully passive downconversion imaging [J. Salman et al, Journal of Optics 23, 054001 (2021)]
    - We built and demonstrated an all-passive imaging system, demonstrating passive frequency conversion of ultraviolet images into the visible without any significant loss of imaging resolution [J. Salman et al, Journal of Optics 23, 054001 (2021)]
    - We designed and demonstrated a fully passive device in the form factor of a pair of glasses that breaks binocular redundancy, with the goal of enhancing the wearer's ability to distinguished metameric spectra. We do note that no human perception experiments were performed [B. Gundlach et al, Scientific Reports 8, 11971 (2018)
    - We demonstrated a new technique, hyperspectral interference tomography, which combines hyperspectral imaging with thin-film modeling to enable rapid nondestructive analysis of biominerals like nacre [J. Salman et al, PNAS 118, e2023623118 (2021)]
    - We developed several metamaterial and metasurface technologies to enable future developments in imaging and focusing, which can hopefully be used in compact vision-enhancement systems. This includes metamaterials that must be described by more than one refractive index simultaneously [Z. Yu et al, Journal of Physics D: Applied Physics 53, 015108 (2020)], tunable metasurface components using graphene nanoribbons [ACS Photonics (J. Siegel et al, ACS Photonics 8, 1277 (2021)], and inverse-design methods using coupled-mode theory to design very large-scale metasurfaces quickly [Zhou et al, ACS Photonics 8, 8 (2021)].
    - We explored laser-light sails, demonstrating a design based on metasurfaces that self-stabilizes in a laser beam, and thus can "ride" the beam [J. Siegel et al, ACS Photonics 6, 8, 2032 (2019)]
    - We deeply engaged with several papers in the literature that suggested that optical forces on nanostructured metallic surfaces can be enhanced beyond the standard radiation-pressure limit, and concluded that this set of literature is not correct. We wrote a Comment to express our view [Feng et al, Physical Review B 105, 207401 (2022)].

- How were the results disseminated to communities of interest? If there is nothing significant to report during this reporting period, state "Nothing to Report."
    - Typical dissemination for an academic researchers, including publications and talks at conferences and seminars
    - Outreach activities include performing a study for NBC 15, a local TV station, on home UV disinfection products at the height of the covid-19 pandemic (2020),

and hosting an SPIE Career Lab Discussion on science dissemination (2021).

- Describe how the results were disseminated to communities of interest for this reporting period. Include any outreach activities that were undertaken to reach members of communities who are not usually aware of these project activities, for the purpose of enhancing public understanding and increasing interest in learning and careers in science, technology, and the humanities.

Impacts

This component is used to describe ways in which the work, findings, and specific products of the project have had an impact during this reporting period. Describe distinctive contributions, major accomplishments, innovations, successes, or any change in practice or behavior that has come about as a result of the project. You can report on the following impact categories, but you are not required to report on all categories. Please only report in the categories that are relevant to your project:

Development of the principal discipline(s) of the project

The research developed during this project will have substantial impact on the development of passive vision-enhancing technologies—technologies that can be used to augment human vision without the use of a power supply, digital logic, circuits, etc. The technologies we developed enable the partitioning of vision to enable higher spectral resolution (colloquially the ability to see more colors), and extend the spectral range that is visible into the ultraviolet, by passively converting images from the ultraviolet to the infrared. We also developed active systems for hyperspectral spectroscopy, in particular developing a new technique to analyze biominerals based on their position-dependent spectra. We also developed a number of auxiliary technologies that may in the future make these technologies more compact and capable, including large-area metasurfaces, materials with multiple refractive indices, and other metasurfaces and metamaterials.

Simultaneously, we also made progress in the calculation and use of optical forces, designing optical metasurfaces that can serve as laser-light sails, and helping understand the best way to calculate optical forces on nanostructured surfaces.

Other disciplines:

Our work on engineering passive vision-enhancing technologies may also be applicable to imaging – for example converting existing inexpensive visible cameras to see over a broader range from the ultraviolet to the infrared. Our technique for large-area nondestructive characterization of layered biominerals – hyperspectral interference tomography – may have a significant impact on the field of biomineral study, as well as the field of bio-inspired materials. Our optical-force work may enable new types of spacecraft based on laser propulsion.

Describe the impact in this reporting period on the development of human resources

Throughout the four years of this project (three years plus no-cost extension), the project provided funding—usually partial—to six students and one postdoc. The one postdoc, Yuzhe Xiao, will soon start a faculty position in Physics at the University of North Texas, which is a minority-serving institution. Bryan Rubio Perez, a student from an underrepresented background, received his MS, and is presently working at Apple. Jad Salman graduated with a PhD, and is working at Honeywell Aerospace. Chenghao Wan graduated with a PhD, and is presently a postdoc at UW-Madison. Other students have not yet graduated. A number of these students have won awards for their research, as described in the narrative below.

Describe the impact on teaching and educational experiences

During this project, Prof. Kats has taught courses in photonics and nanophotonics, including developing online versions of these classes during the covid-19 pandemic, receiving some of the highest teaching evaluations in the department. These materials are broadly useful moving forward.

Describe the impact in this reporting period on physical, institutional, and information resources that form infrastructure.

Nothing major

Impact on society beyond science and technology:

Nothing major

Changes

This is the final report, and there are no more changes to be made.

[In this section, please incorporate any and all changes that you would like your program officers to know about the grant. The principal investigator is reminded that the recipient organization is required to obtain prior written approval from program officers whenever there are significant changes in the project or its direction. Sections may include:

Changes in approach
Describe any changes in approach during the reporting period and reasons for these changes. Remember that significant changes in objectives and scope require prior approval of the agency.

Problems or delays
Describe problems or delays encountered during the reporting period and actions or plans to resolve them.

Expenditure Impacts
Describe changes during the reporting period that may have had a significant impact on expenditures, for example, delays in hiring staff or favorable developments that enable meeting objectives at less cost than anticipated.

Significant changes in the use or care of human subjects, vertebrate animals and/or biohazards
Describe significant deviations, unexpected outcomes, or changes in approved protocols for the use or care of human subjects, vertebrate animals, biohazards, and/or select agents during the reporting period. If required, were these changes approved by the applicable institution committee (or equivalent) and reported to the agency? Also specify the applicable Institutional Review Board/Institutional Animal Care and Use Committee approval dates.

Changes to the primary place of performance from that originally proposed
Identify any change to the primary performance site location identified in the proposal, as originally submitted.]

Technical Updates

[This section will include any and all technical updates that you would like to provide to your program officer. You are encouraged to upload graphs and other visualizations that highlight the work done during this reporting period. Program Officers may request additional information that is specific to your research topics.]

In this section, we will summarize the technical advances achieved during this project.

Passive frequency conversion of ultraviolet images into the visible using perovskite nanocrystals

A core component of the work proposed in the original grant proposal is the passive frequency conversion of images, thus creating a visual aid that expands the range of human vision outside of the visible without using any external power source, digital logic, or any other active component.

The primary challenge of such frequency-conversion imaging is to design a robust optical system that implements a frequency converter but also maintains spatial coherence such that, for example, an incoming ultraviolet beam coming in at a particular angle can be converted into a visible beam moving in the same direction.

Our scheme to accomplished this has been published in the “Emerging Leaders” special issue in the *Journal of Optics* [J. Salman et al, *Journal of Optics* 23, 054001 (2021)], per invitation from the journal editors, and is outlined in Fig. 1. The fundamental idea is an imaging system focused at infinity and designed for direct viewing with human eyes, that includes a frequency-converting film in a conjugate plane to the retina. Light coming in at a particular angle from infinity gets mapped to a point on the frequency-converting medium, and this point is then imaged onto the retina, generating a visible image. This approach is applicable for any frequency-converting medium (e.g., for either down- or upconversion), and can be designed such that a human observe a scene in the visible range and a range outside of the visible simultaneously, enhancing the amount of spectral information available in a scene.

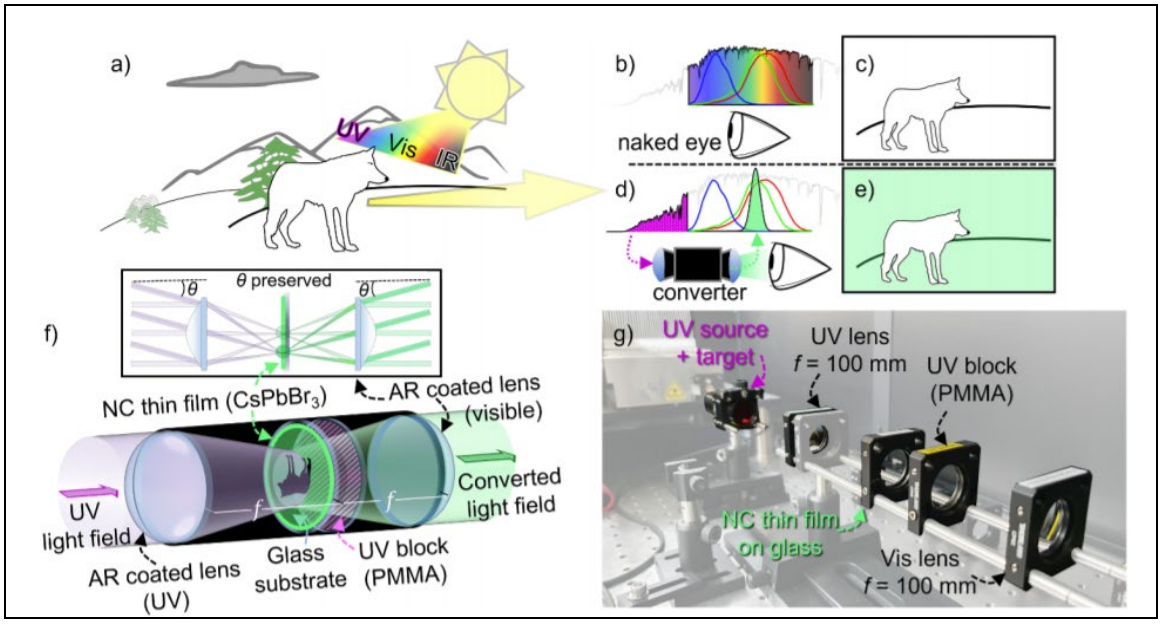

Figure 1: Passive down-conversion imaging. a) An arctic wolf's fur coat scatters and reflects sunlight, which is spectrally broad. However, ultraviolet (UV) frequencies are strongly absorbed by its fur compared to the surrounding snow. To an unaided human eye (b,c), the wolf blends in with the snowy background since human vision is only sensitive to wavelengths within the narrow visible band, 400 – 700 nm (highlighted rainbow region of solar spectrum in the inset), and is limited to three spectral bins with broad overlapping sensitivities (red, green, and blue curves inset b). d) Our device converts ultraviolet light into the visible within a narrow wavelength band (here, in the green) while maintaining the directionality of rays, thus enabling passive frequency-conversion imaging. f) A schematic of our converter system, which uses a thin-film coating of CsPbBr3 nanocrystals (NCs) as the frequency-conversion medium, with the film facing the objective lens. The focal arrangement images far-away scenes with 1:1 magnification. e) An image of our experimental setup with all relevant optical elements labeled. A collimated UV diode (λ = 340 nm, FWHM = 11 nm) is used as our illumination source, with the frequency-converted light centered at 510 nm. Reproduced from J. Salman et al, *Journal of Optics* 23, 054001 (2021).

For this project, we chose to implement a downconversion scheme, since downconversion is inherently simpler to achieve with sufficient efficiency than upconversion (converting one photon to another at a lower energy) is much simpler than having to convert two lower-energy photons into one higher-energy one. Our downconversion setup incorporates ~10 nm cesium lead-halide ($CsPbBr_3$) perovskite nanocrystals synthesized at the Rowland Institute by our collaborator, Daniel Congreve (now at Stanford). The nanocrystals are broadly absorbing across the near-ultraviolet spectrum with a peak in absorption at 365 nm (and relatively broad absorption across the UV in general), and a peak in luminescence at ~510 nm (visible green light, close to the peak of the human-vision sensitivity). The nanocrystals were spun to a 80-nm-thick layer, which we also stabilized to the atmosphere using a thin layer of PMMA. The 80-nm-thick nanocrystal layer is far below the depth of field of the imaging optics (in our demonstration, 10.7 μm), and therefore enables down-conversion imaging at the diffraction limit. It is also almost completely transparent to visible light, and therefore the system can enable simultaneous downconversion imaging and visible imaging (Fig. 2).

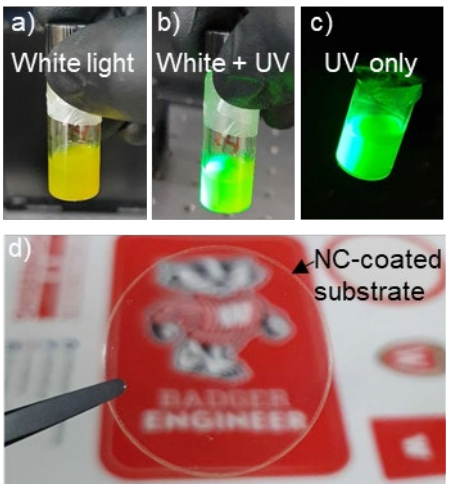

Figure 2. $CsPbBr_3$ downconverter. a) A vial of $CsPbBr_3$ nanocrystals suspended in hexane under white-light illumination, (b) exposed to both white light and ~50 mW of UV light centered at λ = 340 nm, (c) and only under UV illumination. The vibrant green emission of converted light is centered at λ = 510 nm. (d) The 80-nm-thick nanocrystal film deposited on BK7 glass is highly transparent in the visible (the blurry image is because the photo is focused on the sample rather than the background). Reproduced from J. Salman et al, *Journal of Optics* 23, 054001 (2021).

The resulting downconversion imaging as well as simultaneous visible imaging is shown in Fig. 3. We characterized the imaging resolution of our conversion system by imaging a standard 5 mm × 5 mm Air Force resolution target illuminated from the backside with a 50-mW narrow-band ultraviolet light-emitting diode (LED, Thorlabs M340L4), with the output centered at 340 nm and a FWHM of 11 nm. The resolution target was placed 2*f* (200 mm) away from the objective, such that the image magnification on the nanocrystal plane was 1:1. The nanocrystal films were oriented facing the objective side. The eye piece lens was placed 1*f* (100 mm) distance away from the nanocrystal plane such that the converted image was collimated at the output. A digital camera (Nikon D5600) focused to infinity was placed at the end of the eyepiece lens.

Figure 3(b) shows an image of the down-converted resolution target as captured through our setup under a normal white-light ambient background. A separate color logo was placed in the same plane as the resolution target demonstrating how our down-conversion imaging system can simultaneously convert ultraviolet images into the visible while preserving the ability to directly image visible scenery. We then imaged the nanocrystal-only and PMMA-capped samples under ultraviolet illumination, without any ambient lighting (figure 3(d,e)), and compared the images to the resolution target illuminated by a 520-nm-wavelength reference diode (figure 3(c)) to eliminate resolution discrepancies due to chromatic aberrations. As seen in figure 3(c-e) insets, the smallest resolvable feature—defined here as a least a 50% modulation in signal intensity between horizontal lines and spaces (white curves)—was nearly the same between the reference diode and the

nanocrystal-only film (pink dashed boxes, figure 3(c,d) insets). This indicates that our imaging resolution is now limited by the downconversion film.

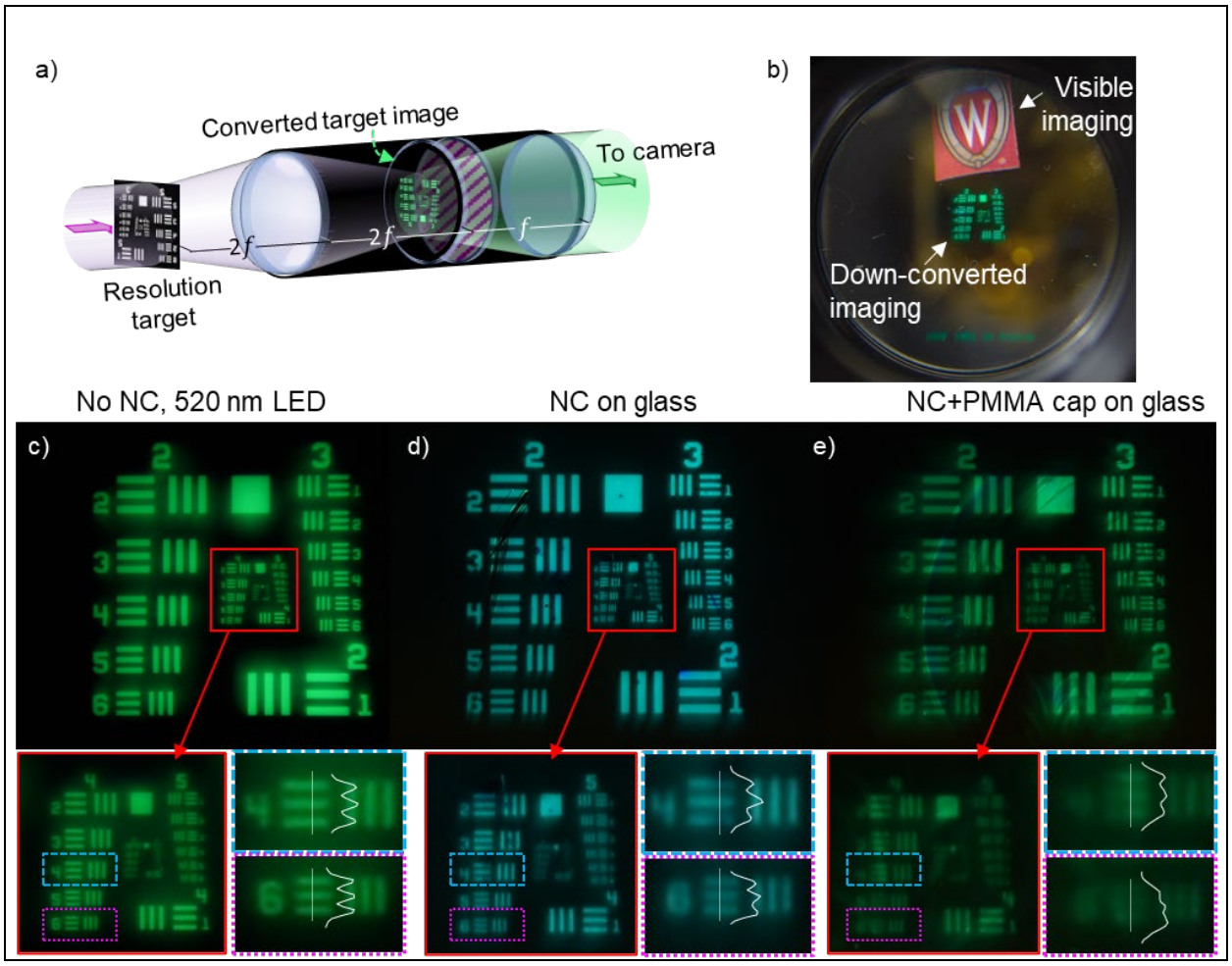

Figure 3: Down-conversion imaging. (a) A schematic of our setup used to image a US Air Force resolution target. The 50-mW ultraviolet source illuminated the backside of the target, which was defined by openings in a chrome mask. The target was placed 2f away from the objective lens to form a 1:1 (unmagnified) image at the nanocrystal plane. (b) A photo through our down-conversion imaging system showing the converted image of the resolution target. The surrounding background is visible due to ambient white light in the scene. A color university logo is placed in the same plane as the resolution target to show our system's ability to simultaneously convert ultraviolet images into the visible and preserve the ability to image the surrounding visible scenery. (c) A baseline image of the resolution target illuminated from behind with a green LED and no nanocrystal (NC) converter in place. Pairs of horizontal and vertical lines and spaces are denoted by group number and element number, e.g., the far lower-right corner set of lines and spaces is labeled as group 2 element 1. (d) Frequency-converted images of the resolution target with the nanocrystal film on glass, and (e) PMMA-capped nanocrystal film on glass samples in place. A shift in the color was noted for the PMMA-capped sample and had a peak PL emission at 520 nm. (c-e insets) the minimum resolvable features for both the baseline image and the nanocrystal-only film are the group-4-element-6 lines (pink inset region) with the horizontal bars being distinguishable (white line = signal intensity profile). The minimum resolvable features of the PMMA-capped nanocrystal film are the group-4-element-6 lines (blue inset region). Only minimal degradation to imaging resolution is noted compared to the baseline performance. Reproduced from J. Salman et al, *Journal of Optics* 23, 054001 (2021).

The conversion efficiency η of our present downconverter is still quiet low, and can be found in Fig. 4(b). The two major factors that determine η are the optics used to collect converted light and the performance of the nanocrystal samples, *i.e.*, the amount of ultraviolet light that is absorbed, the PL quantum yield, and the amount of converted light that can escape, or outcouple, from the material. In Fig. 4(b), we plotted the projected improvements to the system efficiency, η, with various potential enhancements to the down-conversion imaging system compounded together, finding that the efficiency can be pushed into the tens of percent, which is very high, by making significant improvements to the optics and also to the external quantum efficiency of the nanocrystal film. We do believe that all of the improvements projected in Fig. 4(b) are attainable, and will be exploring these in the future.

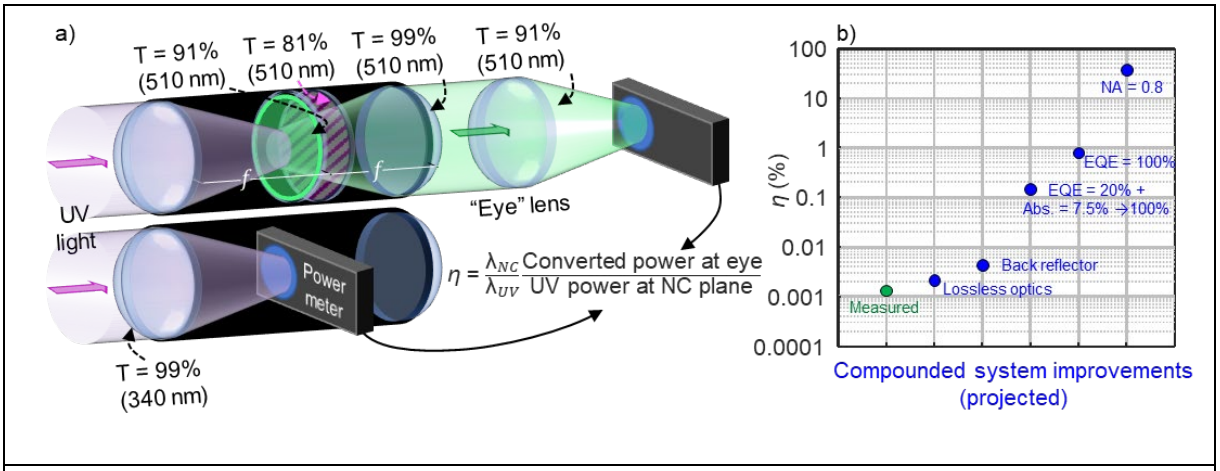

Figure 4: Converter system efficiency. a) The system efficiency, η, is experimentally determined by measuring the power of the converted light at the eye or visible camera, normalized by the ultraviolet power that is focused onto the nanocrystal plane. The transmittance of each optical component is noted for the respective wavelengths. b) The measured η (green dot), and calculated η assuming a variety of improvements to the down-conversion system, compounded at each point. For instance, the use of lossless optics would double η from the measured value. Furthermore, incorporating a back reflector between the nanocrystal structure and objective lens that can redirect backwards-propagating emission—which is typically lost—towards the eyepiece, further doubles of efficiency, and so on. Orders-of-magnitude improvements in system efficiency are possible with increasing external quantum efficiency, enhanced absorption, and the incorporation of larger-NA collecting optics. Reproduced from J. Salman et al, *Journal of Optics* 23, 054001 (2021).

Enhancing vision by breaking binocular redundancy

Another approach we took passively enhance human vision is the breaking of inherent binocular redundancy, providing different spectral content to each eye. This work was published as B. Gundlach et al, *Scientific Reports* 8, 11971 (2018); note that initially AFOSR was not acknowledged by accident, but this has been fixed via an Author Correction.

We fabricated a set of optical filters that "splits" the response of the short-wavelength cone between the two eyes in individuals with typical trichromatic vision, simulating the presence of approximately four distinct cone types (Fig. 5). Such an increase in the number of effective cone types can reduce the prevalence of metamers—pairs of distinct spectra that resolve to the same tristimulus values, and a direct way to see and understand a limitation of the tristimulus human visual system (i.e., one based on three cone types, each with a different spectral sensitivity).

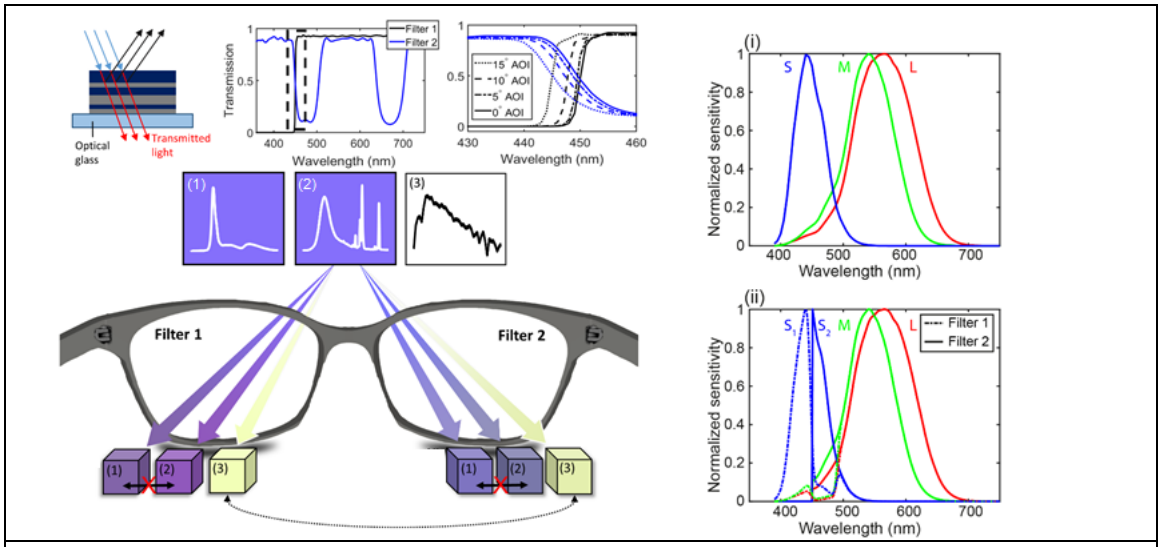

Figure 5. Designing filter-based wearables that break binocular redundancy, and create two effective cone types out of the short-wavelength cone. One filter is a commercial long pass, whereas the other one was custom-designed and manufactured. Right: (i) normalized sensitivities of human color-vision cones. (ii) Effective normalized sensitivities resulting from the product of the filter transmission and effective cone responses. Reproduced from Gundlach et al, *Scientific Reports* 8, 11971 (2018).

Because we did not perform human perception studies, we performed several calculations to justify that an approach that essentially puts different optical filters in front of different eyes would reduce the number of metamers that may be observed. One approach is outlined in Fig. 6. Many pairs of spectra were stochastically generated, counting the number of pairs that would be metamers in the absence of our filter-based visual aid, and the number of metamers that would be present after binocular redundancy is broken with our spectral filters. Though this calculation requires several nontrivial assumptions (described in the manuscript), it seems to imply a reduction of the prevalence of metamers by an order of magnitude.

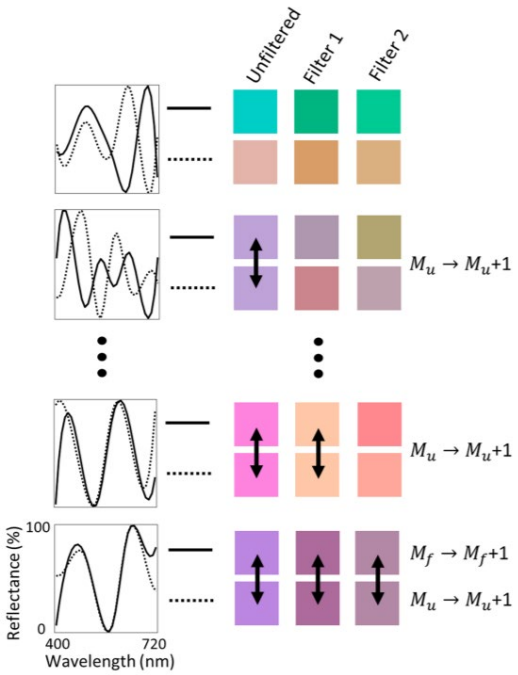

Figure 6. Graphic representation of the Monte-Carlo metamer-reduction calculation using a filter-based vision-enhancement technology, where four pairs of randomly generated spectra are selected as an illustration. Reproduced from Gundlach et al, *Scientific Reports* 8, 11971 (2018).

Hyperspectral interference tomography

At the same time as we were working on enhancing human vision, we also worked on new ways to extract information from spectra acquired using hyperspectral imaging. Specifically, we developed a new metrology technique for layered biominerals based on hyperspectral imaging, in collaboration with the group of Pupa Gilbert at UW-Madison. Our technique is applicable to a variety of layered structures, but we focused on nacre: a biomineral that is formed by various animals in the ocean, and consists of tablets that join to form thin films, separated by thin spacer layers (Fig. 7(a)). The thin-film interference results the well-known iridescent colors of nacreous sea shells (Fig. 7(b-d)). Prof. Gilbert found that the thickness of these tablets correlates well with the temperature of the ocean in which the nacre was formed. Since nacre-forming animals existed from many millions of years ago until now, ancient nacre can be used as a proxy for ancient-ocean temperatures. Furthermore, the study of nacre is important for several subfields in optics and in mechanical engineering; for example, the structure of nacre has inspired materials with enhanced mechanical stability. However, the measurement of mean tablet thickness on a nacre sample is a laborious and expensive process, requiring taking and imaging many cross-sections with electron microscopy or similar technique.

We have developed a rapid and nondestructive technique where a hyperspectral image is acquired of the shell, and the resulting image can be converted into a map of tablet thicknesses across the entire shell (Fig. 7)). This method is related to imaging ellipsometry.

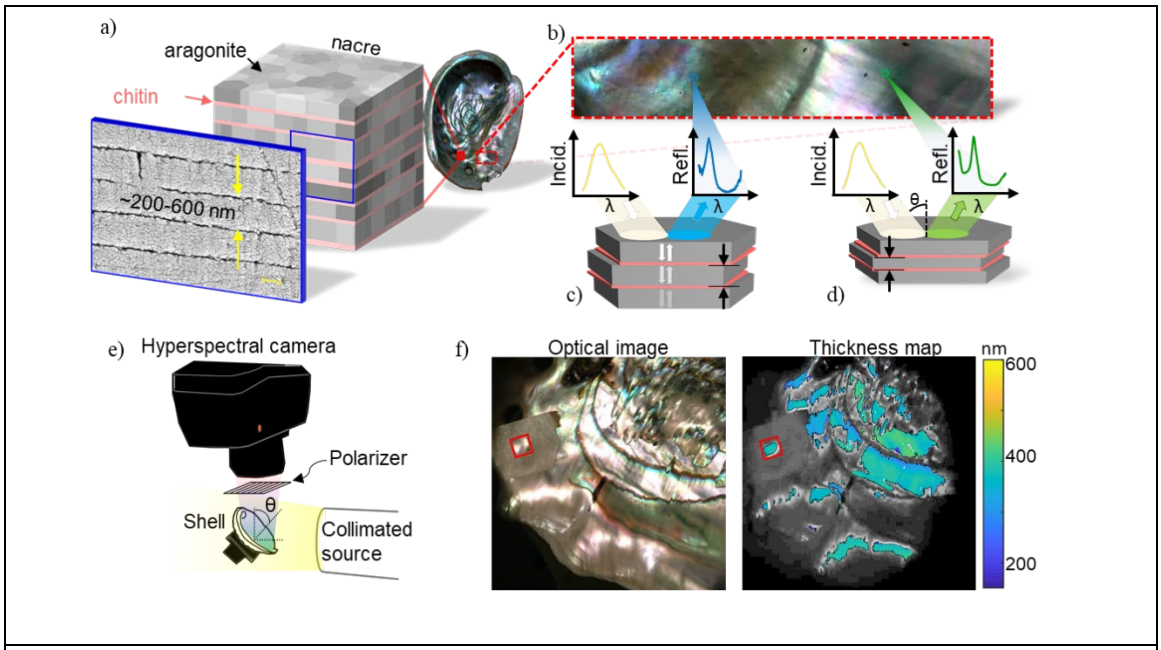

Figure 7. (a) Layered structure of nacre. (b) A close-up color image of the nacre surface shows a variety of colors and nonuniformities. (c, d) Given a broadband white light source illuminating the nacre at a fixed angle of incidence, variations in color are observed due to the difference in average thickness of tablets comprising the stack. (e) Characterization setup: a hyperspectral camera collects predominately specular reflectance data across a sample illuminated by a collimated source at a fixed angle of incidence (θ). (f) Extracting the mean table thickness (TT) across the entire shell. Reproduced from J. Salman et al, *PNAS* 118, e2023623118 (2021)

The technique relies on a thin-film-interference model that is built for every pixel, incorporated the expected stochastic variations, and the experimental data is fit to that model (Fig. 8(a)). The calculations required for fast fitting (after the fact) are substantial: all in all, more than 3 million thin-film calculations were run to generate the data matrix in Fig. 8(c). We captured experimental data from Haliotis rufescens (red abalone), but the method is applicable to a wide variety of both modern and ancient biominerals. We are able to obtain excellent fits between measured data and our model comprising 3 million simulations, resulting in mapping of both the thickness comprising the tablets, and the degree of disorder in the tablets (Fig. 10(d)).

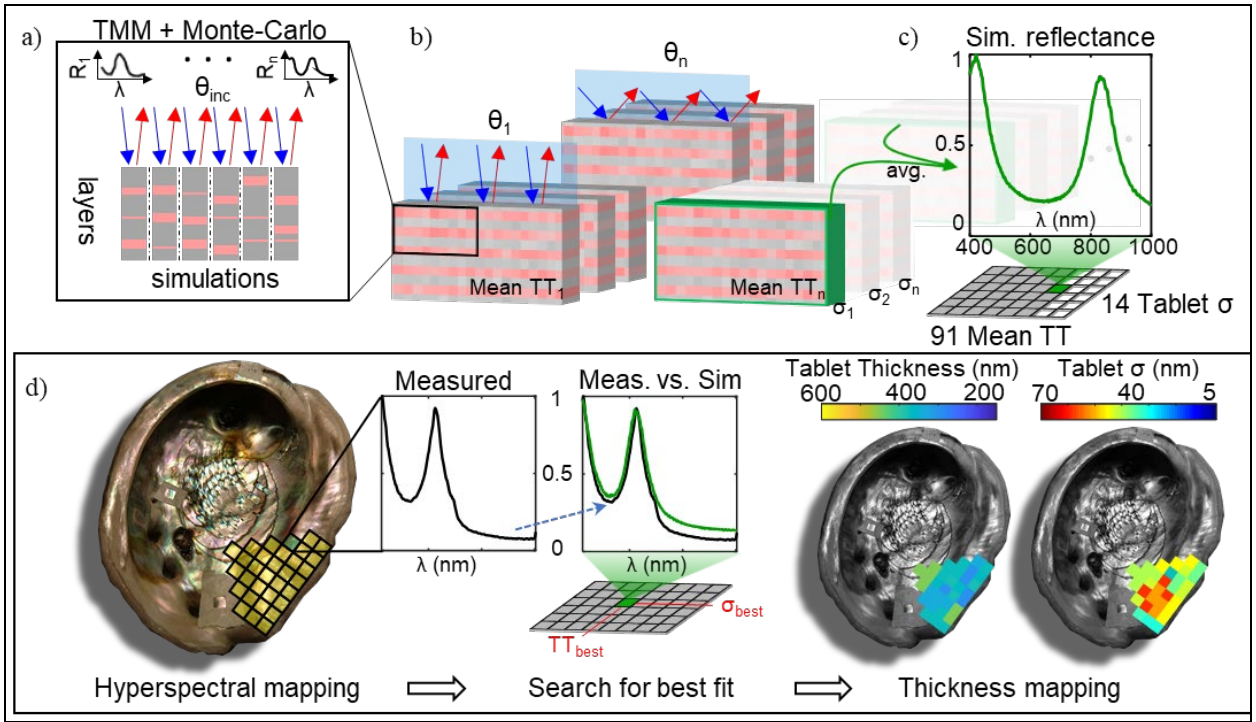

Figure 9. (a-c) Our method for simulating spectra at each pixel of a hyperspectral camera, involving Monte-Carlo sampling and over 3 million simulations to generate the simulation matrix in (c). (d) Fitting experimental hyperspectral data to the simulated data to obtain tablet thickness (TT) and degree of disorder σ. Reproduced from J. Salman et al, *PNAS* 118, e2023623118 (2021)

Since the paper was published in the *Proceedings of the National Academy of Sciences* (J. Salman et al, *PNAS* 118, e2023623118 (2021)), it has been highlighted by many international news outlets, including *Optics & Photonics News*, the *Analytical Scientist*, and the *Science Times*.

Multi-refractive-index metamaterials for focusing and imaging

At the same time, we have been working on new types of metamaterials and metasurfaces that may be used in designing image-converting optical systems such that they can be made more compact or have enhanced functionality. This research has resulted in the theoretical demonstration of a new type of structure that we dubbed the "multi-refractive-index metamaterial" (MRIM), which can be characterized by two or more values of refractive index, even for a particular frequency, incident wave vector, and polarization of light along a symmetry axis of the structure. Effectively, a MRIM behaves as a birefringent material, except a birefringent material acts on two different polarizations whereas a MRIM acts on light with the same polarization.

The paper has now been published as Z. Yu et al, *Journal of Physics D: Applied Physics* 53, 015108 (2020). One example use of MRIMs for imaging systems is shown in Fig. 10. A MRIM

comprising gold and two different dielectrics can be fashioned into the shape of a conventional refractive lens, resulting in two focal spots instead of one. This can be trivially understood by applying the conventional lensmaker's formula, but with two different indices at the same time. In fact, we showed in Fig. 5(c) that the same electric-field pattern is obtained by adding the fields of two conventional refractive lenses with the same indices as the two-index MRIM.

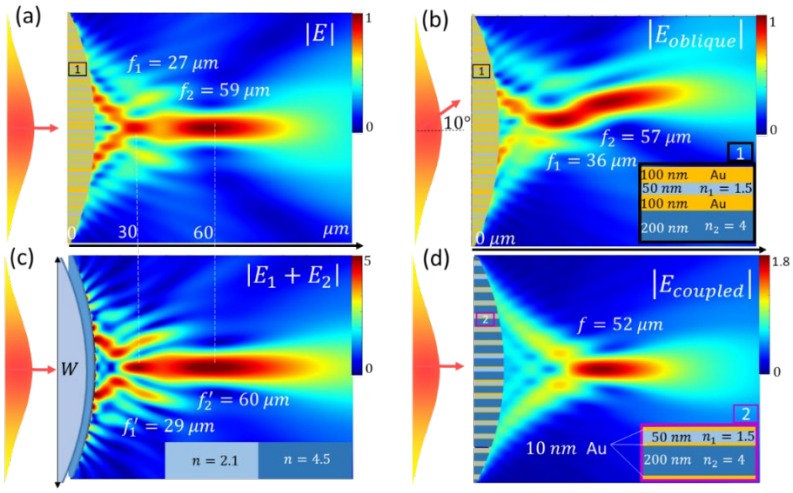

Figure 10. FDTD simulations of light focused by cylindrical lenses. (a) & (b): Two foci are generated by our lens comprising a MRIM with optically thick gold walls, shown in the inset of (b), for (a) normal and (b) oblique incidence at an angle of 10° from free space. (c): A field distribution similar to that in (a) is found by coherently adding the fields from two lenses of the same size and shape as in (a, b), comprising two different homogeneous transparent dielectrics with refractive indices corresponding to the two effective indices of the MRIM. (d): After reducing the gold-layer thickness, only one focus can be observed. Reproduced from Z. Yu et al, *Journal of Physics D* 53, 015108 (2020)

Short-wave, tunable plasmonic resonances

We have been collaborating with the labs of Victor Brar (leading the work), Padma Gopalan, and Michael Arnold at UW-Madison to develop elements that have fast electrical tunability and resonances in the near infrared. We believe that such devices will be relevant to near-infrared upconversion imaging, because they can serve as (1) as tunable masks, and (2) to tune absorption rates of proximal upconverters. Both (1) and (2) can be used to enhance signal-to-noise ratios using lock-in techniques, which will be important for upconversion imaging since it is expected to have lower efficiencies than downconversion imaging.

Our paper on this topic has now been published in *ACS Photonics* (J. Siegel et al, *ACS Photonics* 8, 1277 (2021)).

The basic concept is shown in Fig. 11. The graphene nanoribbons were fabricated based on a technique developed by Padma Gopalan's group, in which a large-scale pattern is generated using phase separation, which can be used as an etch mask to etch the graphene. This allows for the generation of sub-15 nm features over centimeter length scales, which can result in the squeezing of light in such a way that nonlocal and electron-quantization effects can start to play a role.

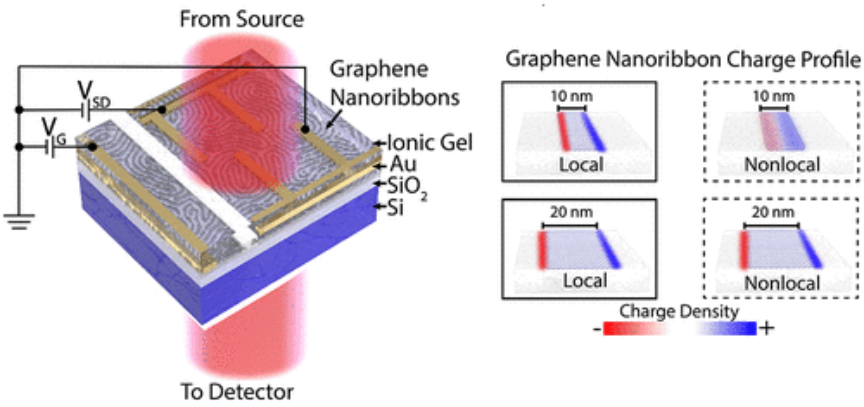

Figure 11. Tunable graphene resonators consisting of gated graphene nanoribbons fabricated in a scalable way using block-copolymer lithography. The nonlocal interactions affect resonator scaling in such a way that the resonance frequency is shifted for the smallest resonators, allowing us to reach frequencies into the SWIR (wavelength down to 2.2 micron). Reproduced from J. Siegel et al, *ACS Photonics* 8, 1277 (2021)).

The results can be seen in Fig. 12, which show resonances in graphene nanoribbons that can be tuned substantially via an applied electric field (Fig. 6(c) – which shows tuning form 5 micron to sub-2.5 micron of the same sample). As described in the paper, the ability to get down to wavelengths close to 2 micron results from nonlocal effects, which begin to be significant for ribbon widths of ~20 nm and smaller. It is likely that further studies will be needed to fully understand and decouple nonlocal effects from the quantum confinement effects. Also, further work will be needed to push the resonances to shorter wavelengths. If the modulation can be made significant in the 1-2 micron regime, then we anticipate that these large-scale inexpensive graphene nanoribbon arrays will be useful as modulators for upconversion imaging, enabling improvements in signal to noise.

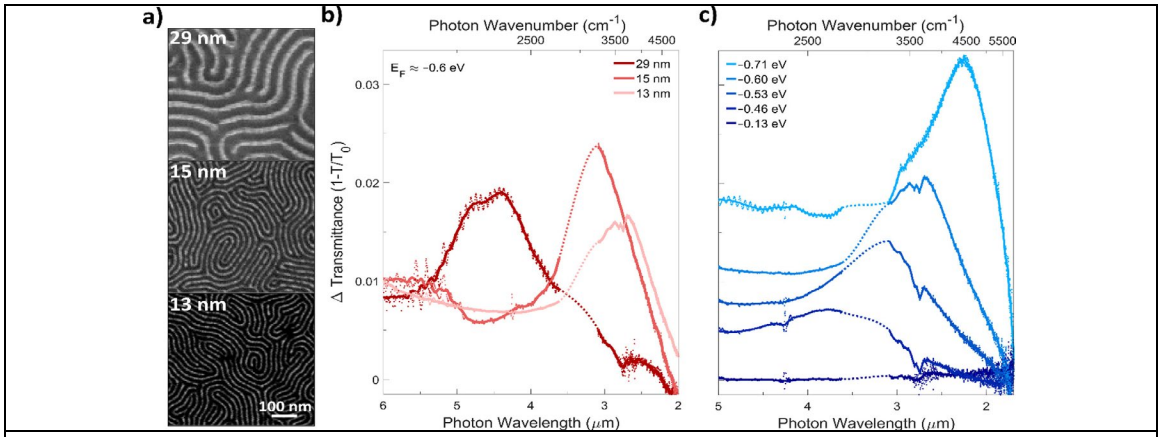

Figure 12. (a) SEM images containing graphene nanoribbons (GNRs) with 29 ± 3, 15 ± 2, and 13 ± 2 nm widths. (b) Differential transmittance through GNRs at a fixed doping level of approximately 0.6 eV normalized to transmittance at the charge neutral point (CNP). (c) Differential transmittance through 13 ± 2 nm wide GNRs as a function of doping level, normalized to transmittance at the CNP. Reproduced from J. Siegel et al, *ACS Photonics* 8, 1277 (2021)).

Inverse design of metasurfaces

The development of vision-enhancement systems that are highly compact will likely require the implementation of large-area flat optics based on optical metasurfaces. As an example, our previously published paper on downconversion imaging [J. Salman et al, *Journal of Optics* 23, 054001 (2021)] utilizes bulk optics with low numerical apertures (NA), whereas low-aberration high-NA optics such as microscope objectives are typically bulky and comprise many refractive optical elements. The use of optical metasurfaces may resolve this tradeoff and enable light and compact optics for vision enhancement and other applications, but existing metasurface design approaches still struggle with the creation of large-area metasurfaces.

To enable large-area metasurface design, we have collaborated with the group of Zongfu Yu at UW-Madison, resulting in a publication titled "Inverse design of metasurfaces based on coupled-mode theory and adjoint optimization" [Zhou et al, ACS Photonics 8, 8 (2021)]. The basic idea is described in Fig. 13. "Traditional" metasurfaces, based on dielectric resonators (or, in earlier designs, metallic resonators) use individual resonators that were optimized and placed in a lookup table; note that I put "traditional" in quotes because significant metasurface design of this type has only been going on for about a decade. The trouble is that when resonators are placed close to other resonators, near-field coupling changes their resonances and scattering properties, and this coupling changes depending on the neighboring resonators, making the optimization problem very challenging. Using coupled-mode theory, we were able to implement an optimization method that took into account coupling of nearby resonators. Thus, the coupling becomes an important design degree of freedom, rather than something that is problematic for metasurface design.

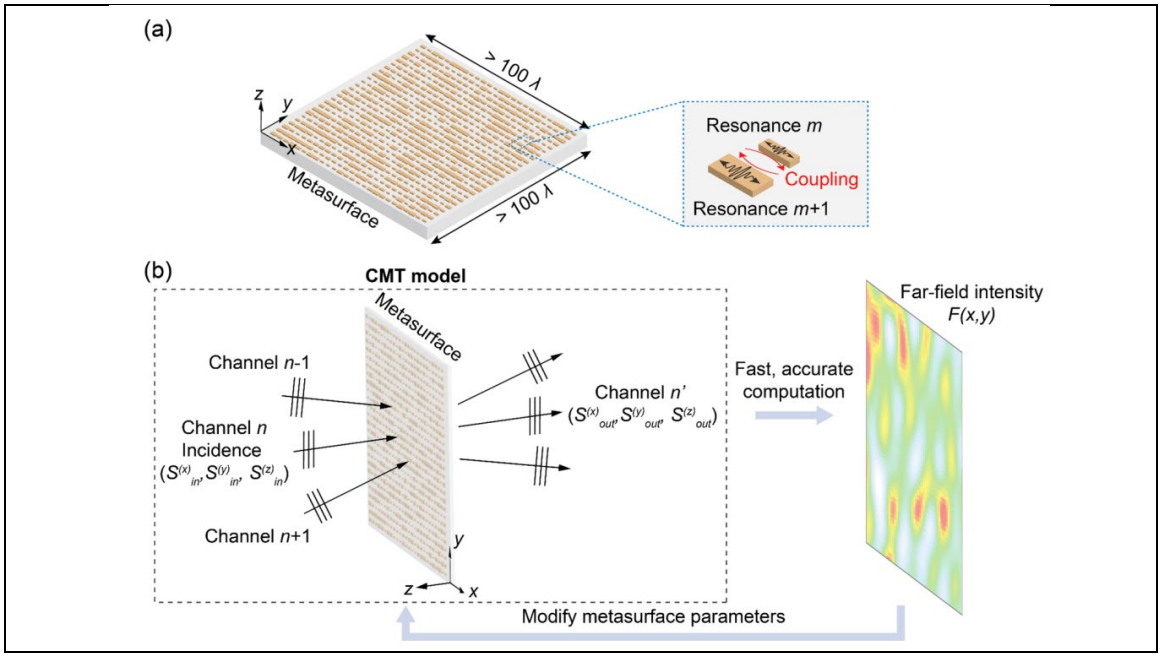

Figure 13. (a) Schematic of a large-scale metasurface containing M optical resonators that are coupled to each other. (b) Schematic of the coupled-mode theory (CMT) framework. The resonators interact with the propagating waves through plane-wave channels. Here, for clarity, we only show incident waves and transmitted waves. The far-field intensity can be accurately and efficiently calculated using coupled-mode theory. From our Zhou et al, *ACS Photonics* 8, 8 (2021).

The resulting performance is shown in Fig. 14. A metalens based on dielectric resonators is designed to have an NA of 0.9, which is quite large, and a size of 10,000 times the operating wavelength. This structure normally has substantial near-field coupling between resonators which absolutely must be accounted for, otherwise the simulations are not accurate at all. Our approach based on CMT and adjoint optimization are able to design and simulate such a lens, and is shown to be many orders of magnitude faster than running even a single full-wave simulation based on the finite element method (FEM) to verify the metasurface performance.

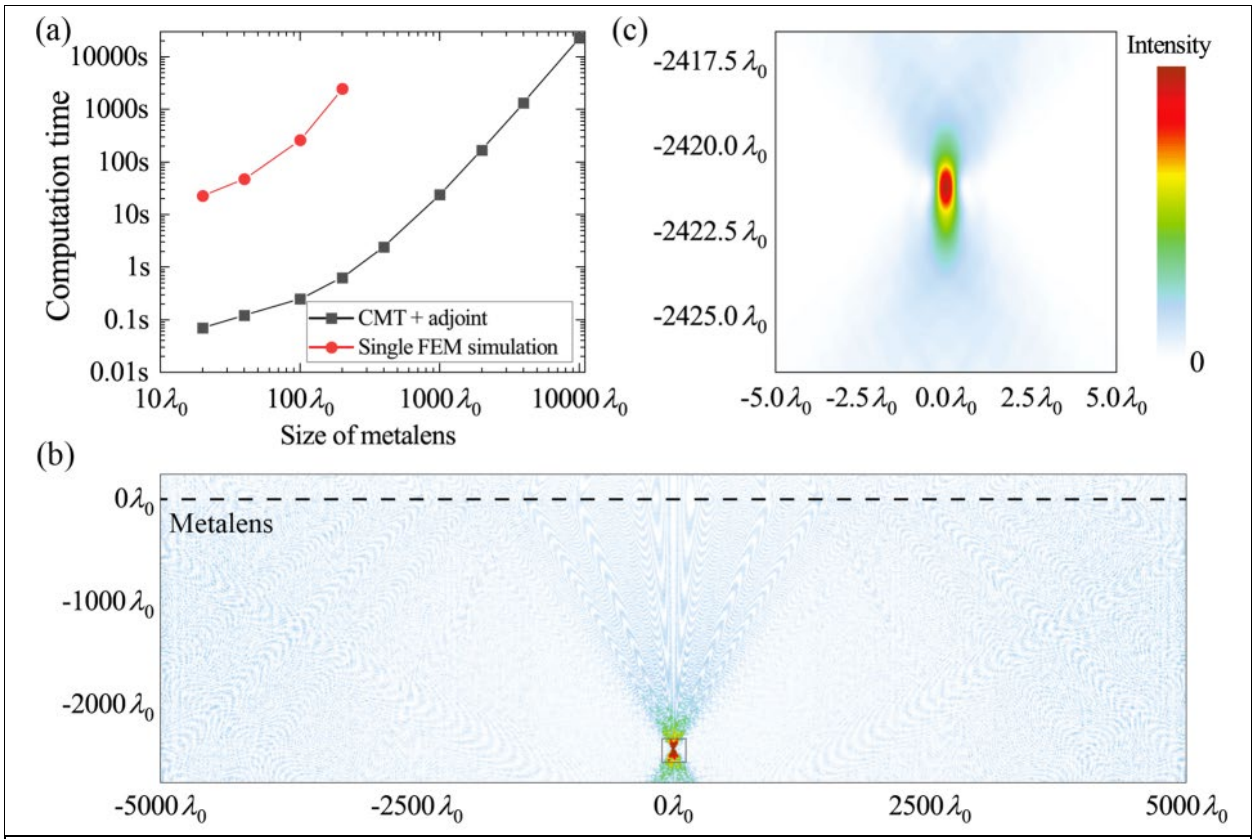

Figure 14. (a) Computation time of single FEM simulations (red circles) and one iteration using our CMT approach (black squares). Our CMT approach is orders of magnitude faster than FEM simulations. (b, c) Intensity distributions of the total field from a designed metalens with a size of $10000\lambda_0$. The designed numerical aperture is 0.9. From our Zhou et al, *ACS Photonics* 8, 8 (2021).

Ultrathin broadband reflective optical limiter

Though we did not discuss them in detail here, some of the simulation/computation techniques used for the aforementioned research directions turned out to be useful for a somewhat different research direction, funded primarily by ONR (but now partially by the present AFOSR project), on reflective optical limiters. This work was recently published as C. Wan et al, *Laser & Photonics* News 15, 2100001 (2021).

Optical limiters are nonlinear devices that feature decreasing transmittance with increasing incident optical intensity, and thus can protect sensitive components from high-intensity illumination. The ideal optical limiter reflects rather than absorbs light in its active ("limiting") state, minimizing risk of damage to the limiter itself. Previous efforts to realize reflective (rather than absorbing) limiters were based on embedding nonlinear layers into relatively thick multilayer photonic structures, resulting in substantial fabrication complexity, reduced speed and, in some instances, limited working bandwidth. In our work, we overcame these tradeoffs using the insulator-to-metal transition (IMT) in vanadium dioxide (VO_2) to achieve intensity-dependent modulation of resonant transmission through aperture antennas. Due to the large change of optical properties across the IMT, low-quality-factor resonators are sufficient to achieve high on–off ratios in the transmittance of the limiter. As a result, our ultrathin reflective limiter (thickness ≈1/100 of the free-space wavelength) is broadband in terms of operating wavelength (>2 μm at 10 μm) and angle of incidence (up to ≈50° away from the normal).

The structure, fabrication flow, and experimental measurements can be found in Fig. 15. The structure is an array of cross-slit apertures in a metal film, which is can be understood as a frequency selective surface (FSS) (or a metasurface), on top of a thin film of VO_2. The basic operating principle is that low-intensity incident light can be transmitted with relatively high transmittance due to resonant transmission through the FSS, but high-intensity light triggers the phase transition in the VO_2, which changes and eventually extinguishes the resonant transmission of the FSS.

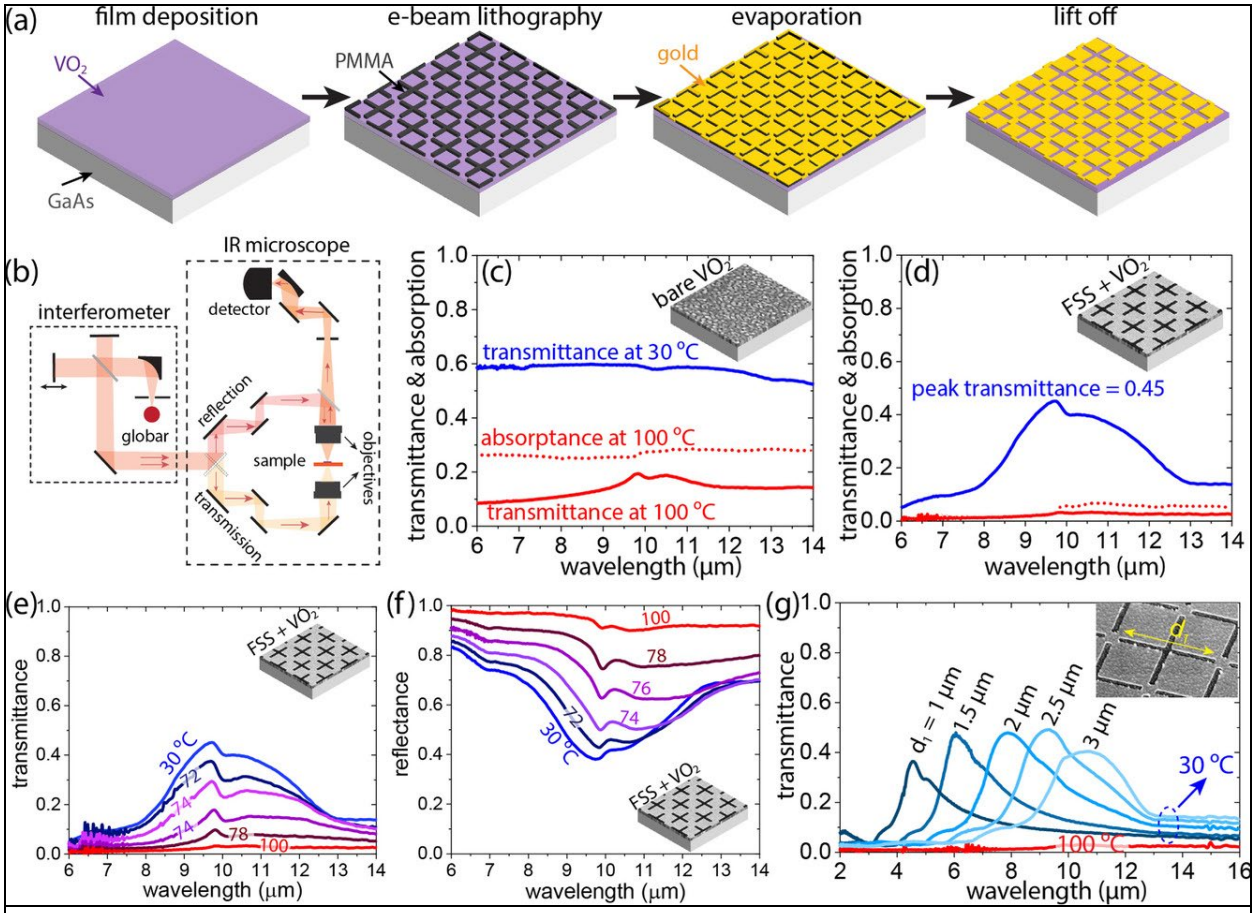

Figure 15. a) Fabrication flow for the reflective limiters based on VO_2 films (phase-transition material) and frequency-selective surfaces. The resulting structures are gold aperture antennas on top of a VO_2 film, on a transparent substrate. b) A schematic of simplified optical path of our transmission and reflection measurements, using an infrared microscope attached to a Fourier-transform spectrometer. c) Transmittance and absorptance spectra of the as-grown VO_2 film, for both insulating (30 °C) and metallic (100 °C) phases. d) Transmittance and absorptance spectra of the FSS-VO_2 limiter at 30 °C (open state) and 100 °C (limiting state). e,f) Transmittance and reflectance measurements of our fabricated FSS-VO_2 limiter when VO2 in its pure insulating phase (30 °C), pure metallic phase (100 °C), and intermediate phases across the IMT (at 72, 74, 76, and 78 °C). g) Measured transmittance of the FSS-VO_2 limiters with aperture lengths d_1 of 1, 1.5, 2, 2.5, and 3 μm, for both open (30 °C) and limiting (100 °C) states. The top surfaces of the inset figures in (c–g) are SEM images of the corresponding fabricated samples. Reproduced from C. Wan et al, *Laser & Photonics* News 15, 2100001 (2021).

The experimental demonstration of our optical limiter operating as a limiter can be found in Fig. 16, which shows limiting behavior using a laser. The limiting behavior is much stronger and occurs at a lower temperature (farther way from the VO_2 transition point) compared to a reference VO_2 film.

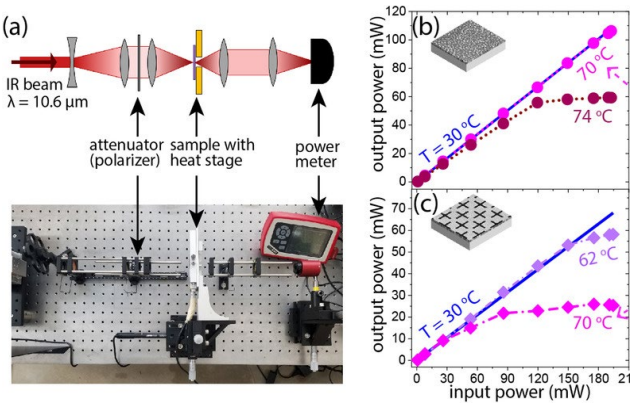

Figure 16. a) Our optical-limiter measurement setup using a continuous-wave CO_2 laser (λ = 10.6 μm) as the light source and a heat stage for thermal biasing. b, c) Power-dependent transmission measurements of (b) the bare VO_2 film and (c) the FSS-VO_2 limiter when they thermally biased at different temperatures. Reproduced from C. Wan et al, *Laser & Photonics* News 15, 2100001 (2021).

This work was featured on the cover of *Laser & Photonics Reviews* (Fig. 17).

Figure 17. Cover of our *Laser & Photonics Reviews*, featuring our recent publication on reflective optical limiters Reproduced from C. Wan et al, *Laser & Photonics* News 15, 2100001 (2021).

Optical forces and light sails

Following discussion with PO Gernot Pomrenke, we have also used this project to explore the science and engineering of optical forces on structured materials, in particular for applications in laser propulsion. Significant interest has built up over the last several years for "laser light sails", which are the laser-driven equivalent of solar sails. Together with the groups of Victor Brar (UW-Madison Physics) and Min Jang (KAIST), we computationally explored designs to make stable sails: that is, laser sails that self-correct their position and orientation if they begin to shift out or turn away from the incident laser beam. This problem is less acute for solar sails since sunlight is not limited to a particular area, but is very acute for laser-light sails.

Our design, recently published as J. Siegel et al, *ACS Photonics* 6, 8, 2032 (2019), is shown schematically in Fig. 18. The design approach is to use dielectric metasurfaces that vary across the sail area, such that light incident on the left side of the sail is reflected toward the right, and light incident on the right part of the sail is incident toward the left, with some special considerations having to do with the reflected wavefronts and the magnitudes of the reflections form each region. Our final design, that we modeled theoretically and also computationally based on Si metasurfaces on SiO_2 substrates at a wavelength of 1.55 um where both material shave very low losses, is referred to as a "inverse cat-eye" (ICE) sail.

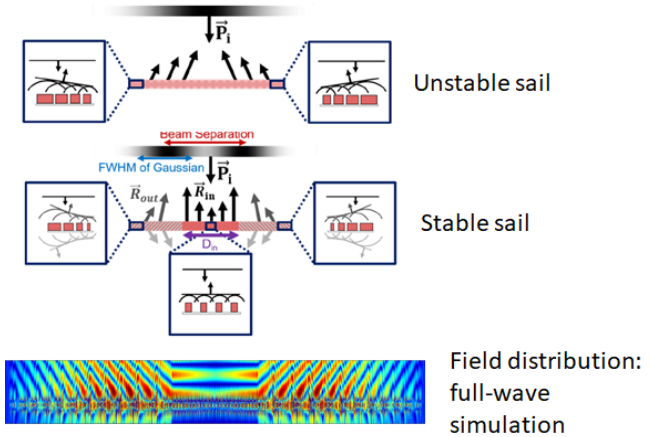

Figure 18. Schematic of our approach to stabilizing laser-light sails. By correctly engineering the magnitude and direction of the reflected beams across the sail, the sail can be stabilized against displacement and rotation, this maintaining its appropriate orientation in the beam. Reproduced from J. Siegel et al, *ACS Photonics* 6, 8, 2032 (2019).

We performed dynamical analysis on the displacement of the sail, δ, and the rotation of the sail θ as a function of time, taking parameters of the driving laser from those being explored for the Breakthrough Starshot initiative (Fig 19). We found that given appropriate design parameters, the ICE sail remains "stable" indefinitely and is able to ride the laser beam as it accelerates. Please note that "stable" here is in quotes, because the sail continues to oscillate as it rides the beam. Additional work is needed to understand how to parametrically cool the sail such that it not only continues to ride the beam but also is truly stable with the oscillation amplitude going to zero. Please also note that we explored both two-dimensional and three-dimensional sails from a

dynamical perspective, but we were only able to simulate the 2D case using full-wave simulations due to the enormous size of the 3D simulations that were ultimately intractable. We anticipate that making and measuring the forces on the sail may be a better future approach than full 3D simulations of the sail.

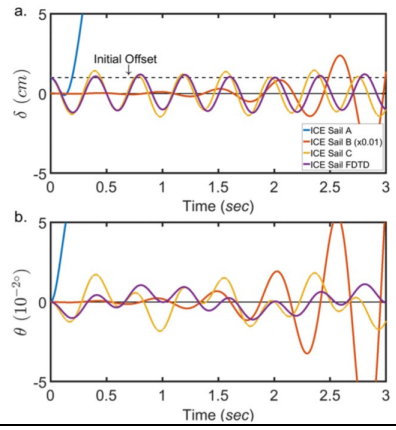

Figure 19. Plots of the displacement (a) and rotation (b) for three different sail and beam combinations over a three second time interval. The parameters for sail size and driving laser beam are taken from the goals of the Breakthrough Starshot initiatives.

Calculation and interpretation of optical forces

The exploration of optical forces for laser-driven propulsion of objects in space has recently become a field of significant interest for the community, driven in part by a recent privately funded effort from the Breakthrough Institute to develop laser sails for propulsion of small craft to Proxima Centauri (disclosure: I am a co-PI, together with Brar and Jang, on a project from the Breakthrough Institute, that was made possible by preliminary work funded on this project). As a result, it has become even more important than before to be able to calculate optical forces from optical field distributions, since the latter can be reliably simulated using various computational techniques such as the finite-difference time-domain (FDTD) method or the finite-element method (FEM).

There have been long-standing debates over how to calculate optical forces from fields. For example, standard textbooks teach that optical forces can be calculated from electromagnetic fields using the Lorentz force law, however other formalisms that are somewhat different exist as well. About a decade ago, Masud Mansuripur (Arizona) began arguing that in certain situations the Lorentz force law gives incorrect results, and that the appropriate formalism to use is the mostly forgotten Einstein-Laub formalism. Debates are still ongoing in the literature about the relative merits of these and other formalisms, and the issue is not settled. To me, the issue is related to the Abraham-Minkowski dilemma, which has to do with how to appropriately assign momentum to light vs to the polarized medium, when light is propagating through a medium.

However, even beyond the debates about force formalisms, there are other issues as well. As I discussed in the previous reports, our group has been looking at a set of papers from Kevin Webb at Purdue University that showed surprising results: that a nanostructured metal surface can be accelerated faster than a flat mirror would be given the same amount of incident light. Specifically, we were looking at the result of Velzen and Webb, Phys. Rev. B 92, 115416 (2015), but there are several other papers following up on this paper with similar conclusions.

One structure that Velzen and Webb explored is schematically shown in Fig. 20: a gold film with periodic slits, and light incident from above the structure from free space. The surprising result of this paper is that the optical forces on a metallic structure such as the periodic structure in Fig. 1 can be much larger than the optical forces on a flat metal mirror (i.e., the same metal structure but with no corrugation). This result appears to be at odds with conservation of momentum, and thus reconciling it with well-established principles relating to the conservation of momentum and the momentum of light in free space will be important: either it will mean a breakdown of very well established physics (much less likely, in our view) or it will give us an understanding of issues with these type of force calculations (much more likely in our view).

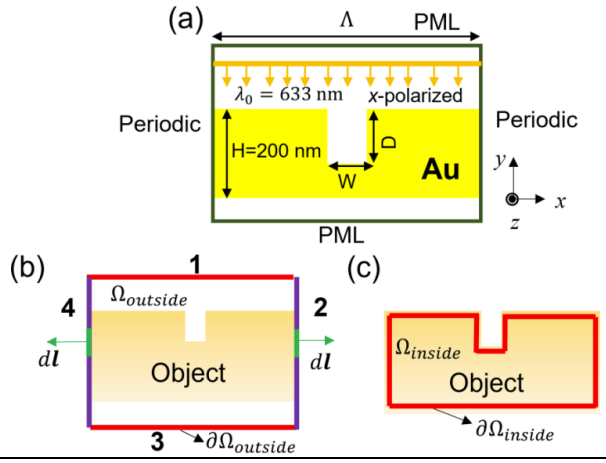

Figure 20. (a) An Au film in free space with periodic slits on the top surface illuminated from the top. (b) and (c) Two choices of the force calculation region Ω for the periodic structure. (b) Outside choice: $\partial\Omega$ consists of two segments in free space and two segments that overlap the periodic boundaries. (c) Inside choice: $\partial\Omega$ is are within the homogeneous object but as close as possible to the boundaries of the object. From our Feng et al, *Physical Review B* 105, 207401 (2022).

After performing our own extensive calculations, we have submitted a Comment to Physical Review B to summarize our findings, which has now been published as Feng et al, *Physical Review B* 105, 207401 (2022). This comment includes our own re-calculation of electromagnetic in the structure (which match those of Velzen and Webb) and force densities using both the Einstein-Laub formalism (which was used by Velzen and Webb) and the Lorentz formalism. We have taken

great care to make sure the calculations are correct, including a significant amount of convergence testing and cross checking. For this structure, all of the field and force-density calculations that we performed are consistent with those of Velzen and Webb. However, the *total forces* we calculated were different from the result of Velzen and Webb, and are not in conflict with any radiation-pressure bounds resulting from the well-established physical concepts of momentum conservation and the momentum of light in free space (Fig. 21).

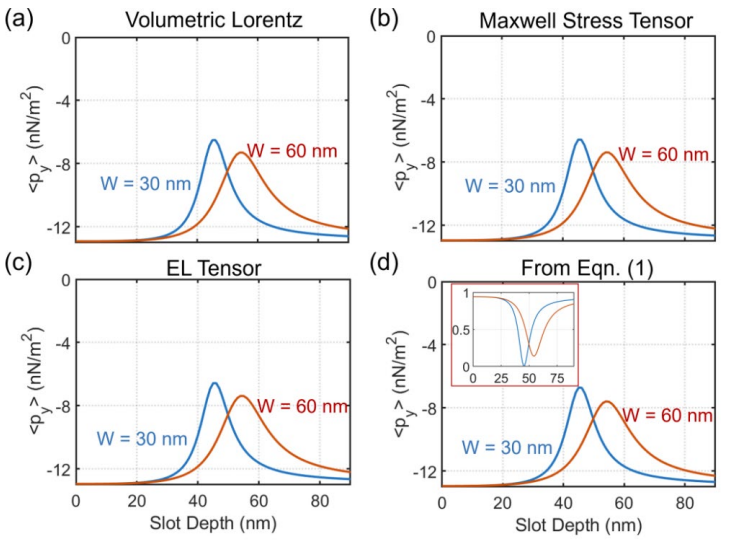

Figure 21. Calculated time-averaged optical pressure as a function of slot depth based on (a) the volumetric Lorentz method, (b) the Maxwell Stress Tensor (MST) method, (c) the Einstein-Laub (EL) tensor method, and (d) a simple radiation-pressure calculation based on the simulated reflectance. In all cases, $\Omega = \Omega_{outside}$. The minus sign means that the direction of the optical force is in the −y direction. The far-field reflectance as a function of slot depth is shown as an inset. From our Feng et al, *Physical Review B* 105, 207401 (2022).

Our understanding is that the difference between our results and those of Velzen and Webb lies in the integration boundaries, when integrating the optical forces. This difference can be seen in Fig. 1: in one case, the integration bound is on the outside of the object (segments 2 and 4 in Fig. 1(b) do not actually count here because they are along periodic boundary conditions, and therefore all contributions along those segments cancel out), and in the other case the integration bound is on the inside of the object, just inside the physical boundary. Though conceptually these two integration bounds should give the same result, they apparently do not because there is a delta-function-like force contribution right at the boundary in both the Lorentz and Einstein-Laub formalisms. This can be seen in Fig. 22 below, showing the large differences between the different choice of integration boundary as a function of simulation mesh size. Better understanding of this (likely nonphysical) delta-function-like force contribution at the interface will help us find a way to accurately treat force densities and forces due to electromagnetic fields.

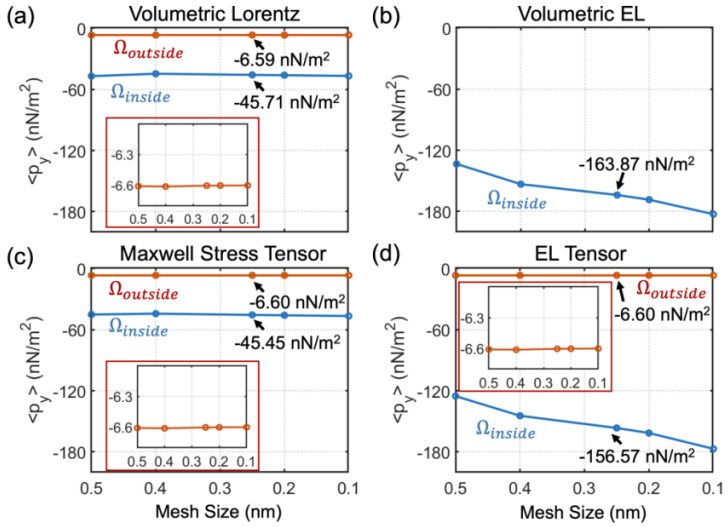

Figure 22. Total time-averaged optical pressure on the structure in Fig. 1 (with W = 30 nm and D = 46 nm), calculated using (a) the volumetric Lorentz method, (b) the volumetric EL method, (c) the MST method, and (d) the EL tensor method with both $\Omega_{outside}$ and Ω_{inside} applied as a function of simulation mesh size. For panels (a), (c), and (d), we show the zoomed-in plots of the results using $\Omega_{outside}$ to demonstrate convergence. From our Feng et al, *Physical Review B* 105, 207401 (2022).

Please note this is a purely scientific disagreement. Our viewpoint is that such debates -- done in a careful and respectful fashion, including the appropriate peer-review channels in established journals -- are helpful to the scientific enterprise and should be encouraged.

AFOSR Deliverable Reporting Format: Final and Interim Reports
Prof Mikhail Kats, Univ of Wisconsin, 2018-2022

This document has been developed to provide Principal Investigators (PIs), co-PIs, and research organizations with:

- A listing of the questions that will be asked in the new AFOSR project reporting format;
- Assistance in planning for the submission of the report

Overview: There are two main sections of the AFOSR Deliverable Report. Section 1 is filled out in Qualtrics, and Section 2 is uploaded by PDF.

- Section 1: Structured Survey Questions in Qualtrics
  - This section captures information in a structured survey format as required by the Research Performance Progress Report Format (RPPR) guidance. Information in this section will include publications, participants, and other intellectual property questions. All questions in this section will be asked within Qualtrics.

- Section 2: Technical Report PDF
  - This section captures unstructured technical information not captured in the above section. PI's will upload PDF reports that contain information on awards, changes to scope, and other technical updates. This PDF upload will be very similar to previous AFOSR report uploads. Please contact your individual program officer if you have further questions about what should be contained in this report.

***Note: The information being asked in this deliverable report is explicitly defined by the official RPPR guidance which can be found here: http://www.nsf.gov/bfa/dias/policy/rppr/index.jsp. We have automated several questions to make the reporting less burdensome on the principal investigator. Your report link, found in the deliverable reminder email, contains individualized information that is specific to your deliverable report. You may edit this information if anything appears to be incorrect.

Section 2: Technical Report PDF Upload

You will be asked to complete the following questions as part of the report documentation section:

- Distribution Statement –Please verify that the report you are about to upload is cleared for public release through your organization's processes and procedures.
- Report Abstract
- Report Document - Upload the Report Document. File must be a PDF. Please do not password protect or secure the PDF. The maximum file size for the Report Document is 100MB.

Regarding the content of the report, we require the following sections in your PDF technical report upload.

Accomplishments

The information provided in this section allows AFOSR to assess whether satisfactory progress has been made during this reporting period. The PI is reminded that the recipient organization is required to obtain prior written approval from the awarding agency grants official whenever there are significant changes in the project or its direction. See agency specific instructions for submission of these requests.

- Research Objectives: Please list the main research objectives of this project
    - [From proposal] The design, fabrication, characterization, and implementation of a fully passive device in the form factor of a pair of glasses that breaks binocular redundancy in the spectral response, enhancing the wearer's ability to distinguish metameric spectra
    - [From proposal] Design and implementation of experimental setups to generate sets of metameric spectra on demand. The development of such setups is necessary for experimental verification of higher-dimensional vision, and for vision psychology experiments that will follow the present project
    - [From proposal] Evaluation and characterization of optical materials and devices for up- and down-conversion of photons into the visible range from the infrared and ultraviolet, respectively at conditions (*i.e.*, intensity, degree of coherence) relevant for vision enhancement.
    - [From proposal] Integration and testing of one or more spectrum-broadening materials and devices described in Objective 3 into an instrument that enables human vision beyond the visible spectral range.
    - [From proposal] Design of an optimal mapping strategy of ultraviolet and near-infrared bands into the visible to maximize the amount of simultaneous information presented to the user
    - [Added in consultation with PO] Development of hyperspectral imaging

technique to analyze biominerals
    - [Added in consultation with PO] Develop better understanding of the calculation of optical forces to enable laser light sails

- Please provide details of accomplishments during this reporting period.
    - We identified an optical material—cesium lead bromide nanocrystals spun onto films and capped for protection—as an excellent candidate for fully passive downconversion imaging [J. Salman et al, Journal of Optics 23, 054001 (2021)]
    - We built and demonstrated an all-passive imaging system, demonstrating passive frequency conversion of ultraviolet images into the visible without any significant loss of imaging resolution [J. Salman et al, Journal of Optics 23, 054001 (2021)]
    - We designed and demonstrated a fully passive device in the form factor of a pair of glasses that breaks binocular redundancy, with the goal of enhancing the wearer's ability to distinguished metameric spectra. We do note that no human perception experiments were performed [B. Gundlach et al, Scientific Reports 8, 11971 (2018)
    - We demonstrated a new technique, hyperspectral interference tomography, which combines hyperspectral imaging with thin-film modeling to enable rapid nondestructive analysis of biominerals like nacre [J. Salman et al, PNAS 118, e2023623118 (2021)]
    - We developed several metamaterial and metasurface technologies to enable future developments in imaging and focusing, which can hopefully be used in compact vision-enhancement systems. This includes metamaterials that must be described by more than one refractive index simultaneously [Z. Yu et al, Journal of Physics D: Applied Physics 53, 015108 (2020)], tunable metasurface components using graphene nanoribbons [ACS Photonics (J. Siegel et al, ACS Photonics 8, 1277 (2021)], and inverse-design methods using coupled-mode theory to design very large-scale metasurfaces quickly [Zhou et al, ACS Photonics 8, 8 (2021)].
    - We explored laser-light sails, demonstrating a design based on metasurfaces that self-stabilizes in a laser beam, and thus can "ride" the beam [J. Siegel et al, ACS Photonics 6, 8, 2032 (2019)]
    - We deeply engaged with several papers in the literature that suggested that optical forces on nanostructured metallic surfaces can be enhanced beyond the standard radiation-pressure limit, and concluded that this set of literature is not correct. We wrote a Comment to express our view [Feng et al, Physical Review B 105, 207401 (2022)].

- How were the results disseminated to communities of interest? If there is nothing significant to report during this reporting period, state "Nothing to Report."
    - Typical dissemination for an academic researchers, including publications and talks at conferences and seminars
    - Outreach activities include performing a study for NBC 15, a local TV station, on home UV disinfection products at the height of the covid-19 pandemic (2020),

and hosting an SPIE Career Lab Discussion on science dissemination (2021).

- Describe how the results were disseminated to communities of interest for this reporting period. Include any outreach activities that were undertaken to reach members of communities who are not usually aware of these project activities, for the purpose of enhancing public understanding and increasing interest in learning and careers in science, technology, and the humanities.

Impacts

This component is used to describe ways in which the work, findings, and specific products of the project have had an impact during this reporting period. Describe distinctive contributions, major accomplishments, innovations, successes, or any change in practice or behavior that has come about as a result of the project. You can report on the following impact categories, but you are not required to report on all categories. Please only report in the categories that are relevant to your project:

Development of the principal discipline(s) of the project

The research developed during this project will have substantial impact on the development of passive vision-enhancing technologies—technologies that can be used to augment human vision without the use of a power supply, digital logic, circuits, etc. The technologies we developed enable the partitioning of vision to enable higher spectral resolution (colloquially the ability to see more colors), and extend the spectral range that is visible into the ultraviolet, by passively converting images from the ultraviolet to the infrared. We also developed active systems for hyperspectral spectroscopy, in particular developing a new technique to analyze biominerals based on their position-dependent spectra. We also developed a number of auxiliary technologies that may in the future make these technologies more compact and capable, including large-area metasurfaces, materials with multiple refractive indices, and other metasurfaces and metamaterials.

Simultaneously, we also made progress in the calculation and use of optical forces, designing optical metasurfaces that can serve as laser-light sails, and helping understand the best way to calculate optical forces on nanostructured surfaces.

Other disciplines:

Our work on engineering passive vision-enhancing technologies may also be applicable to imaging – for example converting existing inexpensive visible cameras to see over a broader range from the ultraviolet to the infrared. Our technique for large-area nondestructive characterization of layered biominerals – hyperspectral interference tomography – may have a significant impact on the field of biomineral study, as well as the field of bio-inspired materials. Our optical-force work may enable new types of spacecraft based on laser propulsion.

Describe the impact in this reporting period on the development of human resources

Throughout the four years of this project (three years plus no-cost extension), the project provided funding—usually partial—to six students and one postdoc. The one postdoc, Yuzhe Xiao, will soon start a faculty position in Physics at the University of North Texas, which is a minority-serving institution. Bryan Rubio Perez, a student from an underrepresented background, received his MS, and is presently working at Apple. Jad Salman graduated with a PhD, and is working at Honeywell Aerospace. Chenghao Wan graduated with a PhD, and is presently a postdoc at UW-Madison. Other students have not yet graduated. A number of these students have won awards for their research, as described in the narrative below.

Describe the impact on teaching and educational experiences

During this project, Prof. Kats has taught courses in photonics and nanophotonics, including developing online versions of these classes during the covid-19 pandemic, receiving some of the highest teaching evaluations in the department. These materials are broadly useful moving forward.

Describe the impact in this reporting period on physical, institutional, and information resources that form infrastructure.

Nothing major

Impact on society beyond science and technology:

Nothing major

Changes

This is the final report, and there are no more changes to be made.

[In this section, please incorporate any and all changes that you would like your program officers to know about the grant. The principal investigator is reminded that the recipient organization is required to obtain prior written approval from program officers whenever there are significant changes in the project or its direction. Sections may include:

Changes in approach
Describe any changes in approach during the reporting period and reasons for these changes. Remember that significant changes in objectives and scope require prior approval of the agency.

Problems or delays
Describe problems or delays encountered during the reporting period and actions or plans to resolve them.

Expenditure Impacts
Describe changes during the reporting period that may have had a significant impact on expenditures, for example, delays in hiring staff or favorable developments that enable meeting objectives at less cost than anticipated.

Significant changes in the use or care of human subjects, vertebrate animals and/or biohazards
Describe significant deviations, unexpected outcomes, or changes in approved protocols for the use or care of human subjects, vertebrate animals, biohazards, and/or select agents during the reporting period. If required, were these changes approved by the applicable institution committee (or equivalent) and reported to the agency? Also specify the applicable Institutional Review Board/Institutional Animal Care and Use Committee approval dates.

Changes to the primary place of performance from that originally proposed
Identify any change to the primary performance site location identified in the proposal, as originally submitted.]

Technical Updates

[This section will include any and all technical updates that you would like to provide to your program officer. You are encouraged to upload graphs and other visualizations that highlight the work done during this reporting period. Program Officers may request additional information that is specific to your research topics.]

In this section, we will summarize the technical advances achieved during this project.

Passive frequency conversion of ultraviolet images into the visible using perovskite nanocrystals

A core component of the work proposed in the original grant proposal is the passive frequency conversion of images, thus creating a visual aid that expands the range of human vision outside of the visible without using any external power source, digital logic, or any other active component.

The primary challenge of such frequency-conversion imaging is to design a robust optical system that implements a frequency converter but also maintains spatial coherence such that, for example, an incoming ultraviolet beam coming in at a particular angle can be converted into a visible beam moving in the same direction.

Our scheme to accomplished this has been published in the “Emerging Leaders” special issue in the *Journal of Optics* [J. Salman et al, *Journal of Optics* 23, 054001 (2021)], per invitation from the journal editors, and is outlined in Fig. 1. The fundamental idea is an imaging system focused at infinity and designed for direct viewing with human eyes, that includes a frequency-converting film in a conjugate plane to the retina. Light coming in at a particular angle from infinity gets mapped to a point on the frequency-converting medium, and this point is then imaged onto the retina, generating a visible image. This approach is applicable for any frequency-converting medium (e.g., for either down- or upconversion), and can be designed such that a human observe a scene in the visible range and a range outside of the visible simultaneously, enhancing the amount of spectral information available in a scene.

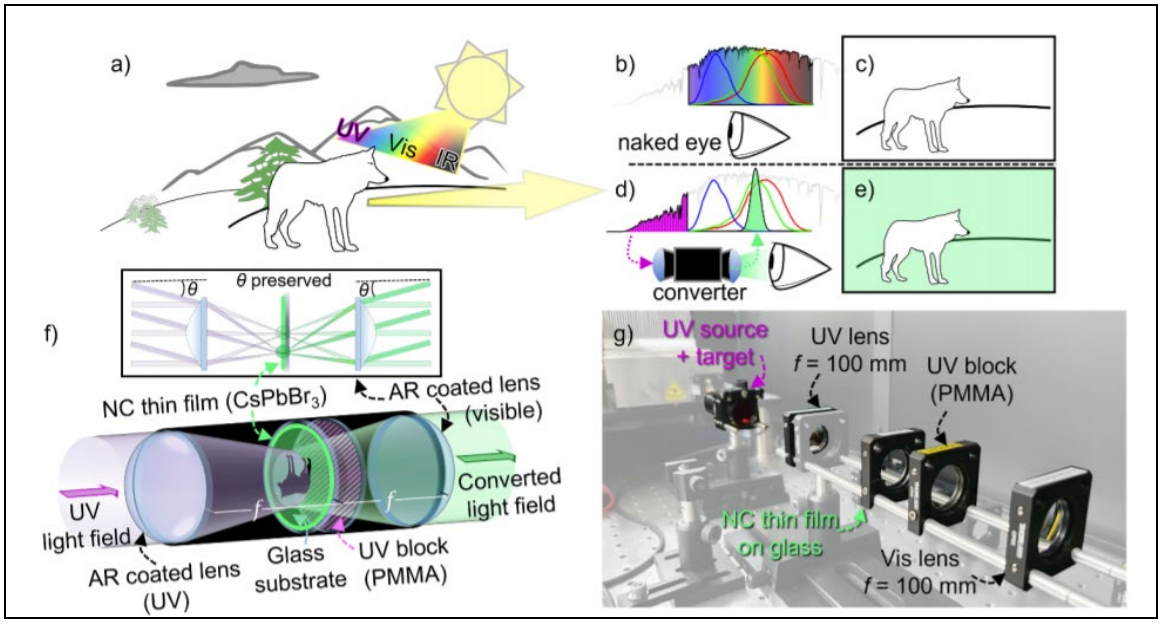

Figure 1: Passive down-conversion imaging. a) An arctic wolf's fur coat scatters and reflects sunlight, which is spectrally broad. However, ultraviolet (UV) frequencies are strongly absorbed by its fur compared to the surrounding snow. To an unaided human eye (b,c), the wolf blends in with the snowy background since human vision is only sensitive to wavelengths within the narrow visible band, 400 – 700 nm (highlighted rainbow region of solar spectrum in the inset), and is limited to three spectral bins with broad overlapping sensitivities (red, green, and blue curves inset b). d) Our device converts ultraviolet light into the visible within a narrow wavelength band (here, in the green) while maintaining the directionality of rays, thus enabling passive frequency-conversion imaging. f) A schematic of our converter system, which uses a thin-film coating of CsPbBr3 nanocrystals (NCs) as the frequency-conversion medium, with the film facing the objective lens. The focal arrangement images far-away scenes with 1:1 magnification. e) An image of our experimental setup with all relevant optical elements labeled. A collimated UV diode (λ = 340 nm, FWHM = 11 nm) is used as our illumination source, with the frequency-converted light centered at 510 nm. Reproduced from J. Salman et al, *Journal of Optics* 23, 054001 (2021).

For this project, we chose to implement a downconversion scheme, since downconversion is inherently simpler to achieve with sufficient efficiency than upconversion (converting one photon to another at a lower energy) is much simpler than having to convert two lower-energy photons into one higher-energy one. Our downconversion setup incorporates ~10 nm cesium lead-halide ($CsPbBr_3$) perovskite nanocrystals synthesized at the Rowland Institute by our collaborator, Daniel Congreve (now at Stanford). The nanocrystals are broadly absorbing across the near-ultraviolet spectrum with a peak in absorption at 365 nm (and relatively broad absorption across the UV in general), and a peak in luminescence at ~510 nm (visible green light, close to the peak of the human-vision sensitivity). The nanocrystals were spun to a 80-nm-thick layer, which we also stabilized to the atmosphere using a thin layer of PMMA. The 80-nm-thick nanocrystal layer is far below the depth of field of the imaging optics (in our demonstration, 10.7 μm), and therefore enables down-conversion imaging at the diffraction limit. It is also almost completely transparent to visible light, and therefore the system can enable simultaneous downconversion imaging and visible imaging (Fig. 2).

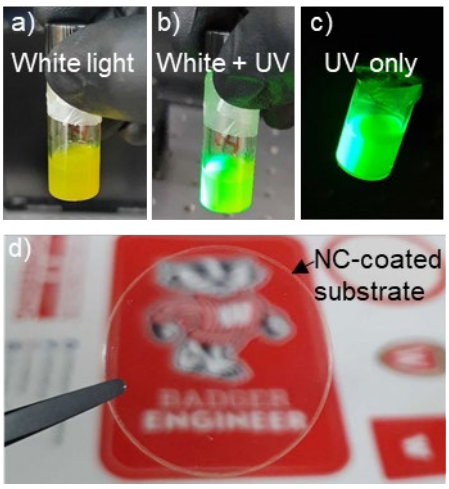

Figure 2. $CsPbBr_3$ downconverter. a) A vial of $CsPbBr_3$ nanocrystals suspended in hexane under white-light illumination, (b) exposed to both white light and ~50 mW of UV light centered at λ = 340 nm, (c) and only under UV illumination. The vibrant green emission of converted light is centered at λ = 510 nm. (d) The 80-nm-thick nanocrystal film deposited on BK7 glass is highly transparent in the visible (the blurry image is because the photo is focused on the sample rather than the background). Reproduced from J. Salman et al, *Journal of Optics* 23, 054001 (2021).

The resulting downconversion imaging as well as simultaneous visible imaging is shown in Fig. 3. We characterized the imaging resolution of our conversion system by imaging a standard 5 mm × 5 mm Air Force resolution target illuminated from the backside with a 50-mW narrow-band ultraviolet light-emitting diode (LED, Thorlabs M340L4), with the output centered at 340 nm and a FWHM of 11 nm. The resolution target was placed 2*f* (200 mm) away from the objective, such that the image magnification on the nanocrystal plane was 1:1. The nanocrystal films were oriented facing the objective side. The eye piece lens was placed 1*f* (100 mm) distance away from the nanocrystal plane such that the converted image was collimated at the output. A digital camera (Nikon D5600) focused to infinity was placed at the end of the eyepiece lens.

Figure 3(b) shows an image of the down-converted resolution target as captured through our setup under a normal white-light ambient background. A separate color logo was placed in the same plane as the resolution target demonstrating how our down-conversion imaging system can simultaneously convert ultraviolet images into the visible while preserving the ability to directly image visible scenery. We then imaged the nanocrystal-only and PMMA-capped samples under ultraviolet illumination, without any ambient lighting (figure 3(d,e)), and compared the images to the resolution target illuminated by a 520-nm-wavelength reference diode (figure 3(c)) to eliminate resolution discrepancies due to chromatic aberrations. As seen in figure 3(c-e) insets, the smallest resolvable feature—defined here as a least a 50% modulation in signal intensity between horizontal lines and spaces (white curves)—was nearly the same between the reference diode and the

nanocrystal-only film (pink dashed boxes, figure 3(c,d) insets). This indicates that our imaging resolution is now limited by the downconversion film.

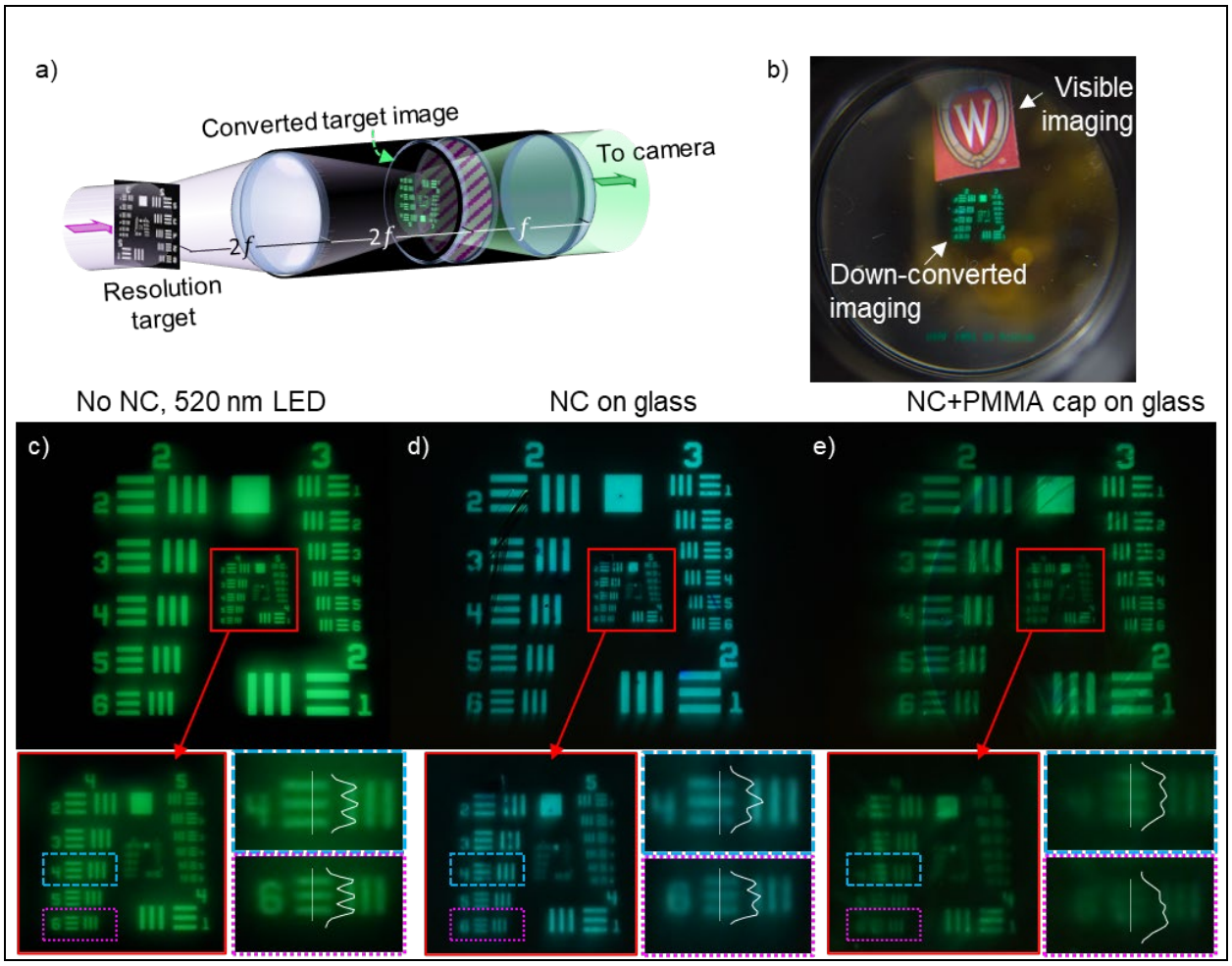

Figure 3: Down-conversion imaging. (a) A schematic of our setup used to image a US Air Force resolution target. The 50-mW ultraviolet source illuminated the backside of the target, which was defined by openings in a chrome mask. The target was placed 2f away from the objective lens to form a 1:1 (unmagnified) image at the nanocrystal plane. (b) A photo through our down-conversion imaging system showing the converted image of the resolution target. The surrounding background is visible due to ambient white light in the scene. A color university logo is placed in the same plane as the resolution target to show our system's ability to simultaneously convert ultraviolet images into the visible and preserve the ability to image the surrounding visible scenery. (c) A baseline image of the resolution target illuminated from behind with a green LED and no nanocrystal (NC) converter in place. Pairs of horizontal and vertical lines and spaces are denoted by group number and element number, e.g., the far lower-right corner set of lines and spaces is labeled as group 2 element 1. (d) Frequency-converted images of the resolution target with the nanocrystal film on glass, and (e) PMMA-capped nanocrystal film on glass samples in place. A shift in the color was noted for the PMMA-capped sample and had a peak PL emission at 520 nm. (c-e insets) the minimum resolvable features for both the baseline image and the nanocrystal-only film are the group-4-element-6 lines (pink inset region) with the horizontal bars being distinguishable (white line = signal intensity profile). The minimum resolvable features of the PMMA-capped nanocrystal film are the group-4-element-6 lines (blue inset region). Only minimal degradation to imaging resolution is noted compared to the baseline performance. Reproduced from J. Salman et al, *Journal of Optics* 23, 054001 (2021).

The conversion efficiency η of our present downconverter is still quiet low, and can be found in Fig. 4(b). The two major factors that determine η are the optics used to collect converted light and the performance of the nanocrystal samples, *i.e.*, the amount of ultraviolet light that is absorbed, the PL quantum yield, and the amount of converted light that can escape, or outcouple, from the material. In Fig. 4(b), we plotted the projected improvements to the system efficiency, η, with various potential enhancements to the down-conversion imaging system compounded together, finding that the efficiency can be pushed into the tens of percent, which is very high, by making significant improvements to the optics and also to the external quantum efficiency of the nanocrystal film. We do believe that all of the improvements projected in Fig. 4(b) are attainable, and will be exploring these in the future.

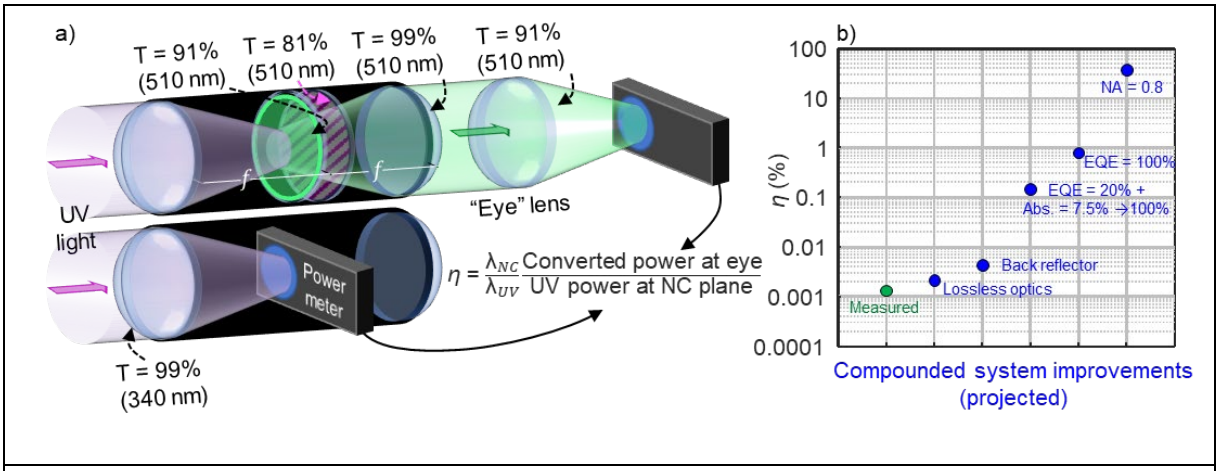

Figure 4: Converter system efficiency. a) The system efficiency, η, is experimentally determined by measuring the power of the converted light at the eye or visible camera, normalized by the ultraviolet power that is focused onto the nanocrystal plane. The transmittance of each optical component is noted for the respective wavelengths. b) The measured η (green dot), and calculated η assuming a variety of improvements to the down-conversion system, compounded at each point. For instance, the use of lossless optics would double η from the measured value. Furthermore, incorporating a back reflector between the nanocrystal structure and objective lens that can redirect backwards-propagating emission—which is typically lost—towards the eyepiece, further doubles of efficiency, and so on. Orders-of-magnitude improvements in system efficiency are possible with increasing external quantum efficiency, enhanced absorption, and the incorporation of larger-NA collecting optics. Reproduced from J. Salman et al, *Journal of Optics* 23, 054001 (2021).

Enhancing vision by breaking binocular redundancy

Another approach we took passively enhance human vision is the breaking of inherent binocular redundancy, providing different spectral content to each eye. This work was published as B. Gundlach et al, *Scientific Reports* 8, 11971 (2018); note that initially AFOSR was not acknowledged by accident, but this has been fixed via an Author Correction.

We fabricated a set of optical filters that "splits" the response of the short-wavelength cone between the two eyes in individuals with typical trichromatic vision, simulating the presence of approximately four distinct cone types (Fig. 5). Such an increase in the number of effective cone types can reduce the prevalence of metamers—pairs of distinct spectra that resolve to the same tristimulus values, and a direct way to see and understand a limitation of the tristimulus human visual system (i.e., one based on three cone types, each with a different spectral sensitivity).

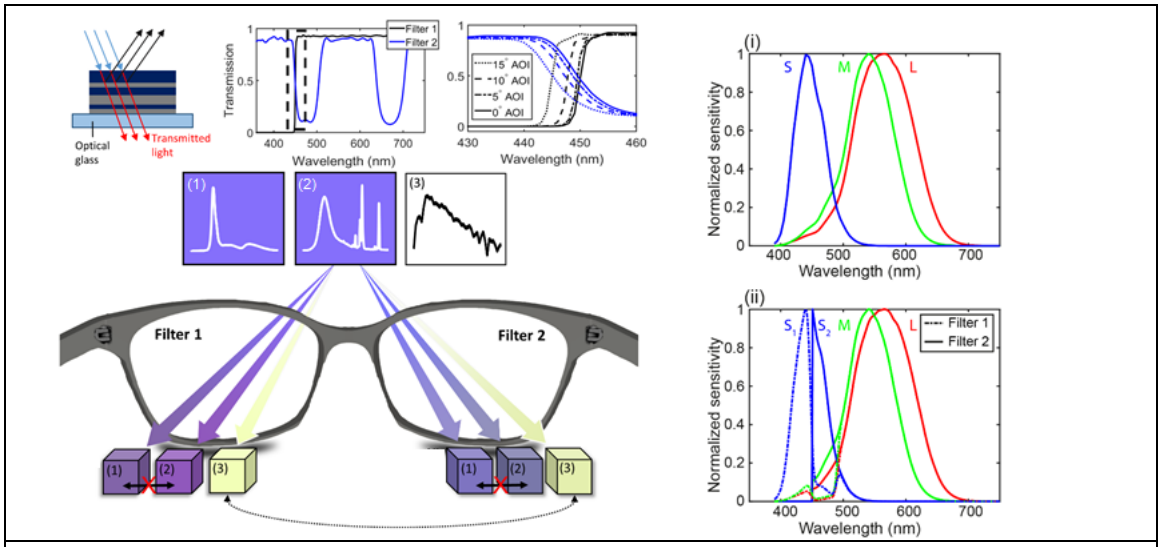

Figure 5. Designing filter-based wearables that break binocular redundancy, and create two effective cone types out of the short-wavelength cone. One filter is a commercial long pass, whereas the other one was custom-designed and manufactured. Right: (i) normalized sensitivities of human color-vision cones. (ii) Effective normalized sensitivities resulting from the product of the filter transmission and effective cone responses. Reproduced from Gundlach et al, *Scientific Reports* 8, 11971 (2018).

Because we did not perform human perception studies, we performed several calculations to justify that an approach that essentially puts different optical filters in front of different eyes would reduce the number of metamers that may be observed. One approach is outlined in Fig. 6. Many pairs of spectra were stochastically generated, counting the number of pairs that would be metamers in the absence of our filter-based visual aid, and the number of metamers that would be present after binocular redundancy is broken with our spectral filters. Though this calculation requires several nontrivial assumptions (described in the manuscript), it seems to imply a reduction of the prevalence of metamers by an order of magnitude.

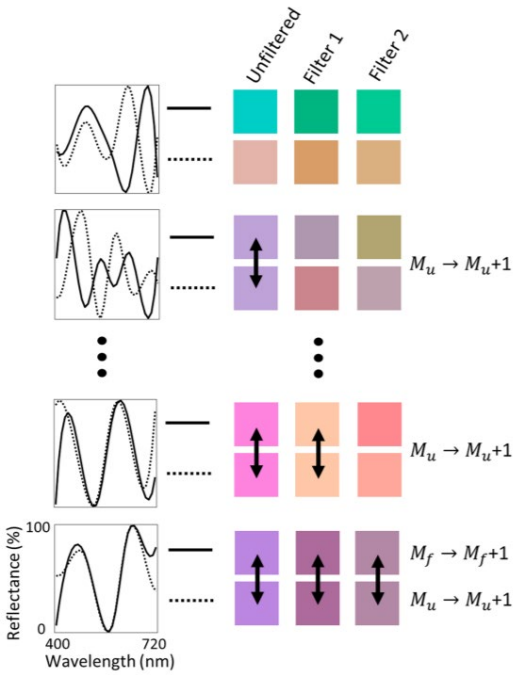

Figure 6. Graphic representation of the Monte-Carlo metamer-reduction calculation using a filter-based vision-enhancement technology, where four pairs of randomly generated spectra are selected as an illustration. Reproduced from Gundlach et al, *Scientific Reports* 8, 11971 (2018).

Hyperspectral interference tomography

At the same time as we were working on enhancing human vision, we also worked on new ways to extract information from spectra acquired using hyperspectral imaging. Specifically, we developed a new metrology technique for layered biominerals based on hyperspectral imaging, in collaboration with the group of Pupa Gilbert at UW-Madison. Our technique is applicable to a variety of layered structures, but we focused on nacre: a biomineral that is formed by various animals in the ocean, and consists of tablets that join to form thin films, separated by thin spacer layers (Fig. 7(a)). The thin-film interference results the well-known iridescent colors of nacreous sea shells (Fig. 7(b-d)). Prof. Gilbert found that the thickness of these tablets correlates well with the temperature of the ocean in which the nacre was formed. Since nacre-forming animals existed from many millions of years ago until now, ancient nacre can be used as a proxy for ancient-ocean temperatures. Furthermore, the study of nacre is important for several subfields in optics and in mechanical engineering; for example, the structure of nacre has inspired materials with enhanced mechanical stability. However, the measurement of mean tablet thickness on a nacre sample is a laborious and expensive process, requiring taking and imaging many cross-sections with electron microscopy or similar technique.

We have developed a rapid and nondestructive technique where a hyperspectral image is acquired of the shell, and the resulting image can be converted into a map of tablet thicknesses across the entire shell (Fig. 7)). This method is related to imaging ellipsometry.

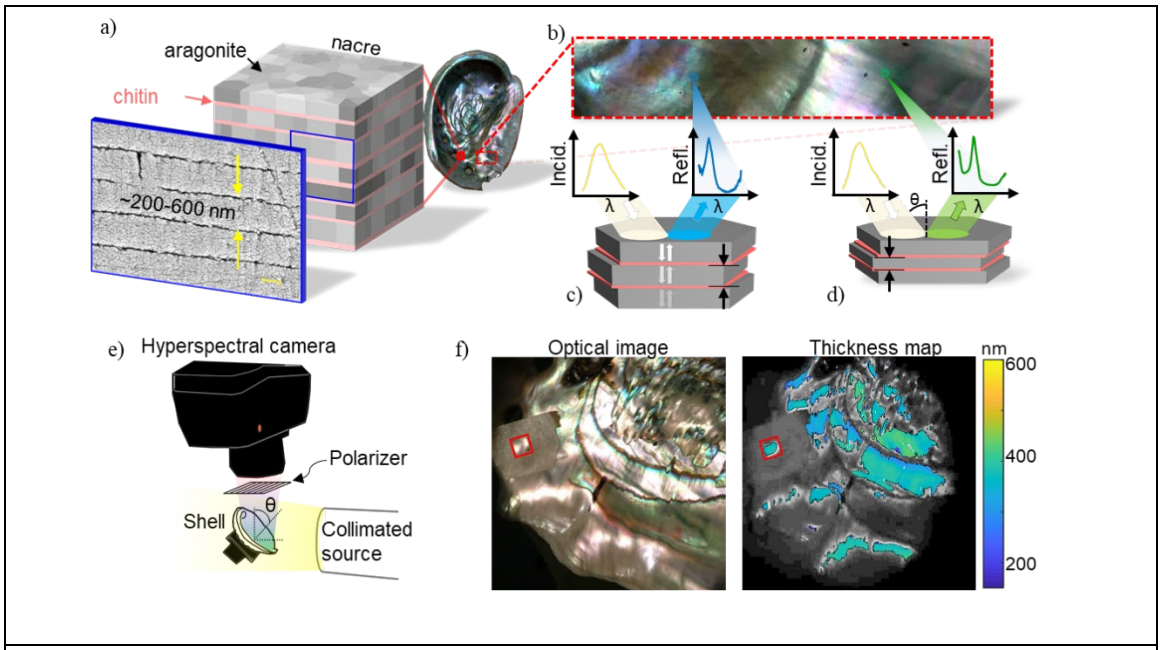

Figure 7. (a) Layered structure of nacre. (b) A close-up color image of the nacre surface shows a variety of colors and nonuniformities. (c, d) Given a broadband white light source illuminating the nacre at a fixed angle of incidence, variations in color are observed due to the difference in average thickness of tablets comprising the stack. (e) Characterization setup: a hyperspectral camera collects predominately specular reflectance data across a sample illuminated by a collimated source at a fixed angle of incidence (θ). (f) Extracting the mean table thickness (TT) across the entire shell. Reproduced from J. Salman et al, *PNAS* 118, e2023623118 (2021)

The technique relies on a thin-film-interference model that is built for every pixel, incorporated the expected stochastic variations, and the experimental data is fit to that model (Fig. 8(a)). The calculations required for fast fitting (after the fact) are substantial: all in all, more than 3 million thin-film calculations were run to generate the data matrix in Fig. 8(c). We captured experimental data from Haliotis rufescens (red abalone), but the method is applicable to a wide variety of both modern and ancient biominerals. We are able to obtain excellent fits between measured data and our model comprising 3 million simulations, resulting in mapping of both the thickness comprising the tablets, and the degree of disorder in the tablets (Fig. 10(d)).

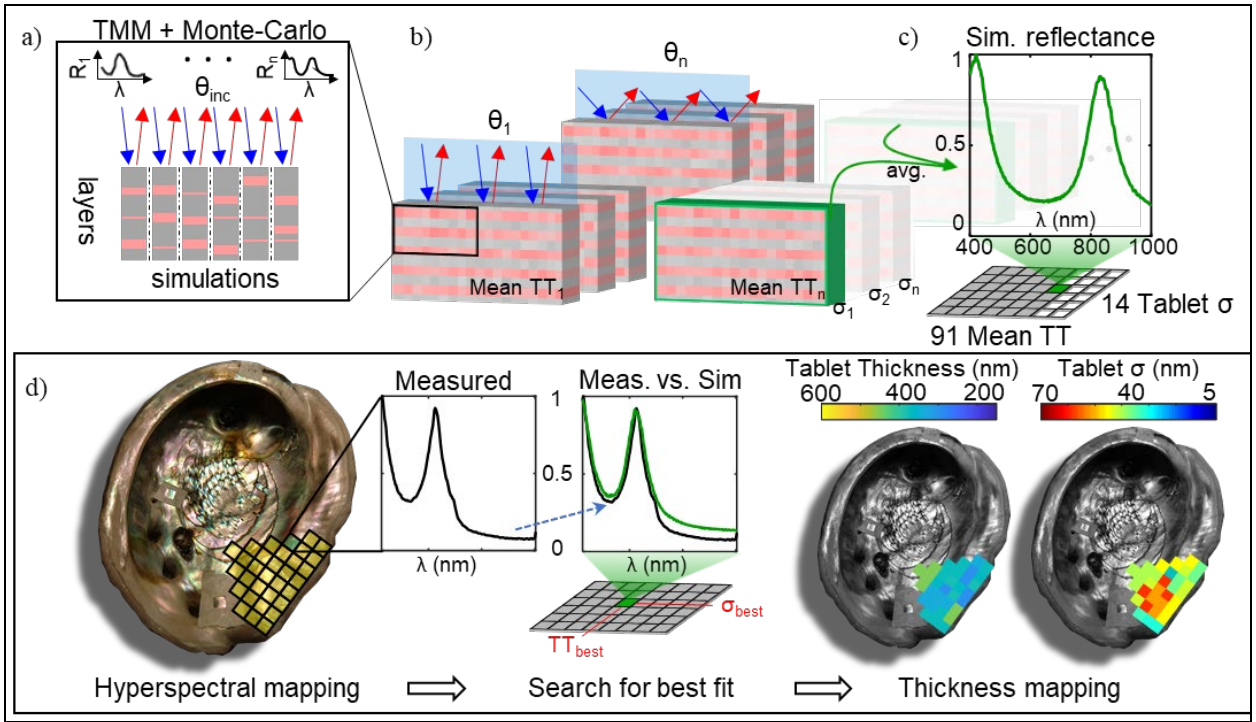

Figure 9. (a-c) Our method for simulating spectra at each pixel of a hyperspectral camera, involving Monte-Carlo sampling and over 3 million simulations to generate the simulation matrix in (c). (d) Fitting experimental hyperspectral data to the simulated data to obtain tablet thickness (TT) and degree of disorder σ. Reproduced from J. Salman et al, *PNAS* 118, e2023623118 (2021)

Since the paper was published in the *Proceedings of the National Academy of Sciences* (J. Salman et al, *PNAS* 118, e2023623118 (2021)), it has been highlighted by many international news outlets, including *Optics & Photonics News*, the *Analytical Scientist*, and the *Science Times*.

Multi-refractive-index metamaterials for focusing and imaging

At the same time, we have been working on new types of metamaterials and metasurfaces that may be used in designing image-converting optical systems such that they can be made more compact or have enhanced functionality. This research has resulted in the theoretical demonstration of a new type of structure that we dubbed the "multi-refractive-index metamaterial" (MRIM), which can be characterized by two or more values of refractive index, even for a particular frequency, incident wave vector, and polarization of light along a symmetry axis of the structure. Effectively, a MRIM behaves as a birefringent material, except a birefringent material acts on two different polarizations whereas a MRIM acts on light with the same polarization.

The paper has now been published as Z. Yu et al, *Journal of Physics D: Applied Physics* 53, 015108 (2020). One example use of MRIMs for imaging systems is shown in Fig. 10. A MRIM

comprising gold and two different dielectrics can be fashioned into the shape of a conventional refractive lens, resulting in two focal spots instead of one. This can be trivially understood by applying the conventional lensmaker's formula, but with two different indices at the same time. In fact, we showed in Fig. 5(c) that the same electric-field pattern is obtained by adding the fields of two conventional refractive lenses with the same indices as the two-index MRIM.

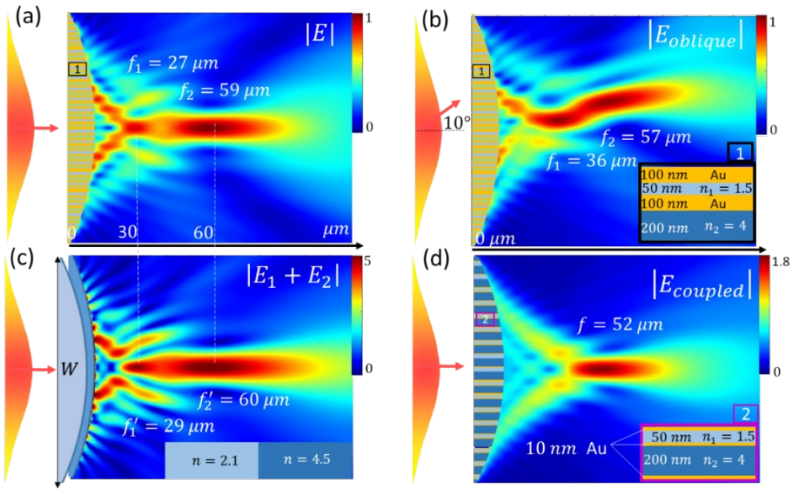

Figure 10. FDTD simulations of light focused by cylindrical lenses. (a) & (b): Two foci are generated by our lens comprising a MRIM with optically thick gold walls, shown in the inset of (b), for (a) normal and (b) oblique incidence at an angle of 10° from free space. (c): A field distribution similar to that in (a) is found by coherently adding the fields from two lenses of the same size and shape as in (a, b), comprising two different homogeneous transparent dielectrics with refractive indices corresponding to the two effective indices of the MRIM. (d): After reducing the gold-layer thickness, only one focus can be observed. Reproduced from Z. Yu et al, *Journal of Physics D* 53, 015108 (2020)

Short-wave, tunable plasmonic resonances

We have been collaborating with the labs of Victor Brar (leading the work), Padma Gopalan, and Michael Arnold at UW-Madison to develop elements that have fast electrical tunability and resonances in the near infrared. We believe that such devices will be relevant to near-infrared upconversion imaging, because they can serve as (1) as tunable masks, and (2) to tune absorption rates of proximal upconverters. Both (1) and (2) can be used to enhance signal-to-noise ratios using lock-in techniques, which will be important for upconversion imaging since it is expected to have lower efficiencies than downconversion imaging.

Our paper on this topic has now been published in *ACS Photonics* (J. Siegel et al, *ACS Photonics* 8, 1277 (2021)).

The basic concept is shown in Fig. 11. The graphene nanoribbons were fabricated based on a technique developed by Padma Gopalan's group, in which a large-scale pattern is generated using phase separation, which can be used as an etch mask to etch the graphene. This allows for the generation of sub-15 nm features over centimeter length scales, which can result in the squeezing of light in such a way that nonlocal and electron-quantization effects can start to play a role.

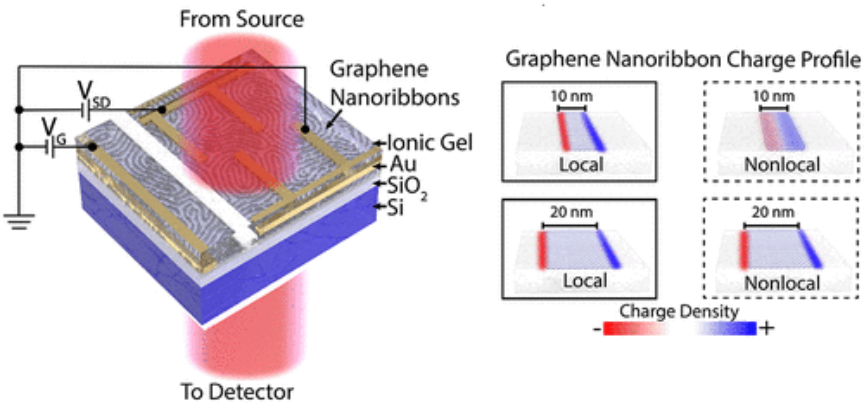

Figure 11. Tunable graphene resonators consisting of gated graphene nanoribbons fabricated in a scalable way using block-copolymer lithography. The nonlocal interactions affect resonator scaling in such a way that the resonance frequency is shifted for the smallest resonators, allowing us to reach frequencies into the SWIR (wavelength down to 2.2 micron). Reproduced from J. Siegel et al, *ACS Photonics* 8, 1277 (2021)).

The results can be seen in Fig. 12, which show resonances in graphene nanoribbons that can be tuned substantially via an applied electric field (Fig. 6(c) – which shows tuning form 5 micron to sub-2.5 micron of the same sample). As described in the paper, the ability to get down to wavelengths close to 2 micron results from nonlocal effects, which begin to be significant for ribbon widths of ~20 nm and smaller. It is likely that further studies will be needed to fully understand and decouple nonlocal effects from the quantum confinement effects. Also, further work will be needed to push the resonances to shorter wavelengths. If the modulation can be made significant in the 1-2 micron regime, then we anticipate that these large-scale inexpensive graphene nanoribbon arrays will be useful as modulators for upconversion imaging, enabling improvements in signal to noise.

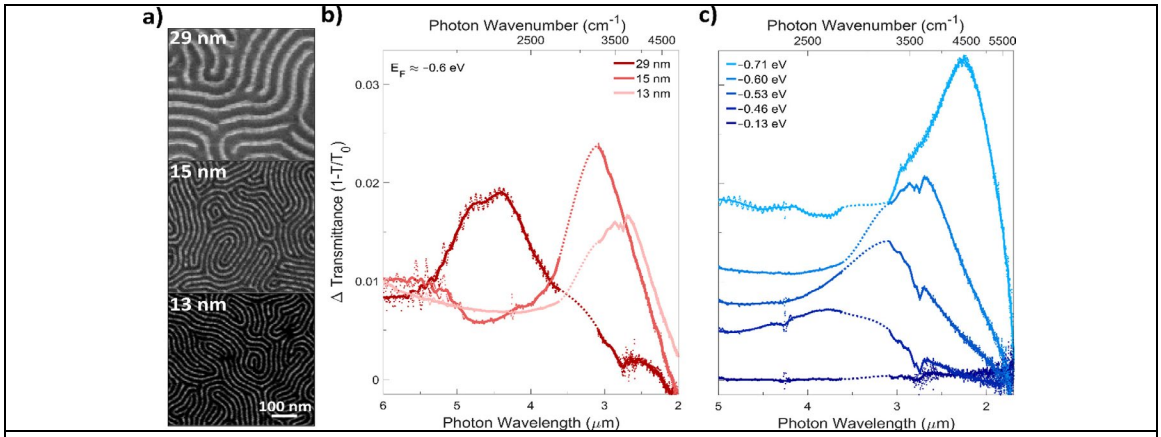

Figure 12. (a) SEM images containing graphene nanoribbons (GNRs) with 29 ± 3, 15 ± 2, and 13 ± 2 nm widths. (b) Differential transmittance through GNRs at a fixed doping level of approximately 0.6 eV normalized to transmittance at the charge neutral point (CNP). (c) Differential transmittance through 13 ± 2 nm wide GNRs as a function of doping level, normalized to transmittance at the CNP. Reproduced from J. Siegel et al, *ACS Photonics* 8, 1277 (2021)).

Inverse design of metasurfaces

The development of vision-enhancement systems that are highly compact will likely require the implementation of large-area flat optics based on optical metasurfaces. As an example, our previously published paper on downconversion imaging [J. Salman et al, *Journal of Optics* 23, 054001 (2021)] utilizes bulk optics with low numerical apertures (NA), whereas low-aberration high-NA optics such as microscope objectives are typically bulky and comprise many refractive optical elements. The use of optical metasurfaces may resolve this tradeoff and enable light and compact optics for vision enhancement and other applications, but existing metasurface design approaches still struggle with the creation of large-area metasurfaces.

To enable large-area metasurface design, we have collaborated with the group of Zongfu Yu at UW-Madison, resulting in a publication titled "Inverse design of metasurfaces based on coupled-mode theory and adjoint optimization" [Zhou et al, ACS Photonics 8, 8 (2021)]. The basic idea is described in Fig. 13. "Traditional" metasurfaces, based on dielectric resonators (or, in earlier designs, metallic resonators) use individual resonators that were optimized and placed in a lookup table; note that I put "traditional" in quotes because significant metasurface design of this type has only been going on for about a decade. The trouble is that when resonators are placed close to other resonators, near-field coupling changes their resonances and scattering properties, and this coupling changes depending on the neighboring resonators, making the optimization problem very challenging. Using coupled-mode theory, we were able to implement an optimization method that took into account coupling of nearby resonators. Thus, the coupling becomes an important design degree of freedom, rather than something that is problematic for metasurface design.

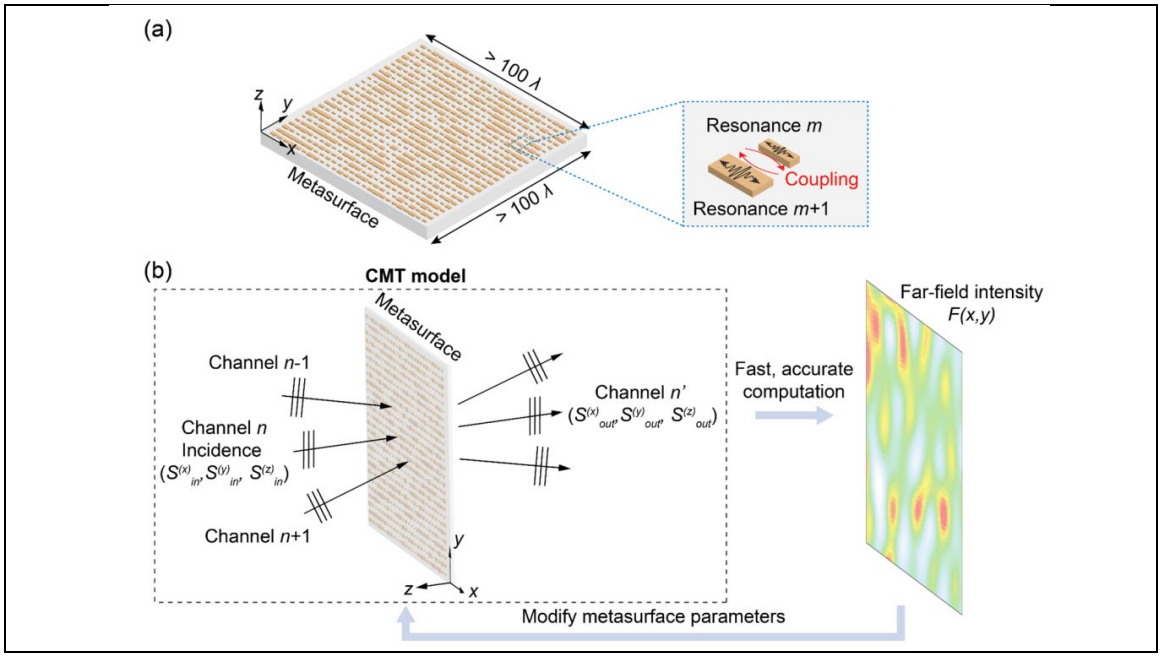

Figure 13. (a) Schematic of a large-scale metasurface containing M optical resonators that are coupled to each other. (b) Schematic of the coupled-mode theory (CMT) framework. The resonators interact with the propagating waves through plane-wave channels. Here, for clarity, we only show incident waves and transmitted waves. The far-field intensity can be accurately and efficiently calculated using coupled-mode theory. From our Zhou et al, *ACS Photonics* 8, 8 (2021).

The resulting performance is shown in Fig. 14. A metalens based on dielectric resonators is designed to have an NA of 0.9, which is quite large, and a size of 10,000 times the operating wavelength. This structure normally has substantial near-field coupling between resonators which absolutely must be accounted for, otherwise the simulations are not accurate at all. Our approach based on CMT and adjoint optimization are able to design and simulate such a lens, and is shown to be many orders of magnitude faster than running even a single full-wave simulation based on the finite element method (FEM) to verify the metasurface performance.

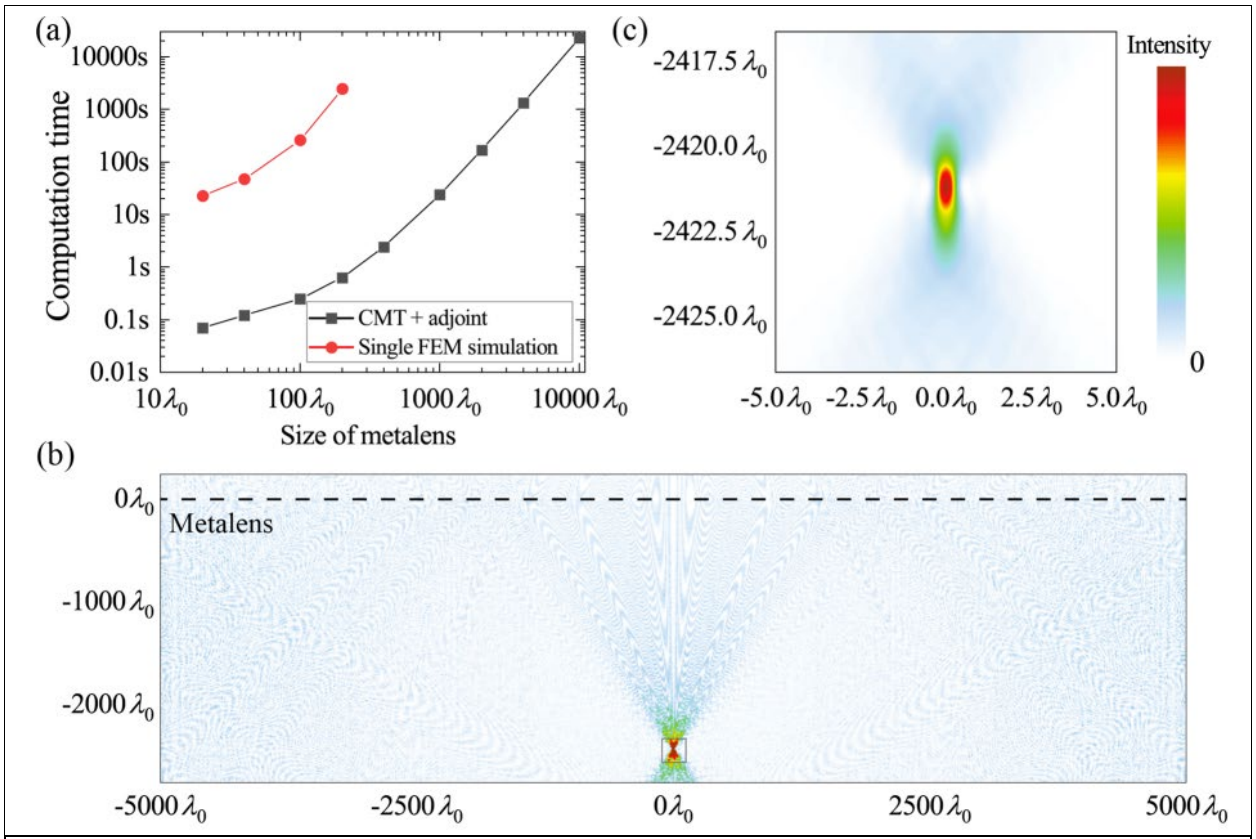

Figure 14. (a) Computation time of single FEM simulations (red circles) and one iteration using our CMT approach (black squares). Our CMT approach is orders of magnitude faster than FEM simulations. (b, c) Intensity distributions of the total field from a designed metalens with a size of $10000\lambda_0$. The designed numerical aperture is 0.9. From our Zhou et al, *ACS Photonics* 8, 8 (2021).

Ultrathin broadband reflective optical limiter

Though we did not discuss them in detail here, some of the simulation/computation techniques used for the aforementioned research directions turned out to be useful for a somewhat different research direction, funded primarily by ONR (but now partially by the present AFOSR project), on reflective optical limiters. This work was recently published as C. Wan et al, *Laser & Photonics* News 15, 2100001 (2021).

Optical limiters are nonlinear devices that feature decreasing transmittance with increasing incident optical intensity, and thus can protect sensitive components from high-intensity illumination. The ideal optical limiter reflects rather than absorbs light in its active ("limiting") state, minimizing risk of damage to the limiter itself. Previous efforts to realize reflective (rather than absorbing) limiters were based on embedding nonlinear layers into relatively thick multilayer photonic structures, resulting in substantial fabrication complexity, reduced speed and, in some instances, limited working bandwidth. In our work, we overcame these tradeoffs using the insulator-to-metal transition (IMT) in vanadium dioxide (VO_2) to achieve intensity-dependent modulation of resonant transmission through aperture antennas. Due to the large change of optical properties across the IMT, low-quality-factor resonators are sufficient to achieve high on–off ratios in the transmittance of the limiter. As a result, our ultrathin reflective limiter (thickness ≈1/100 of the free-space wavelength) is broadband in terms of operating wavelength (>2 μm at 10 μm) and angle of incidence (up to ≈50° away from the normal).

The structure, fabrication flow, and experimental measurements can be found in Fig. 15. The structure is an array of cross-slit apertures in a metal film, which is can be understood as a frequency selective surface (FSS) (or a metasurface), on top of a thin film of VO_2. The basic operating principle is that low-intensity incident light can be transmitted with relatively high transmittance due to resonant transmission through the FSS, but high-intensity light triggers the phase transition in the VO_2, which changes and eventually extinguishes the resonant transmission of the FSS.

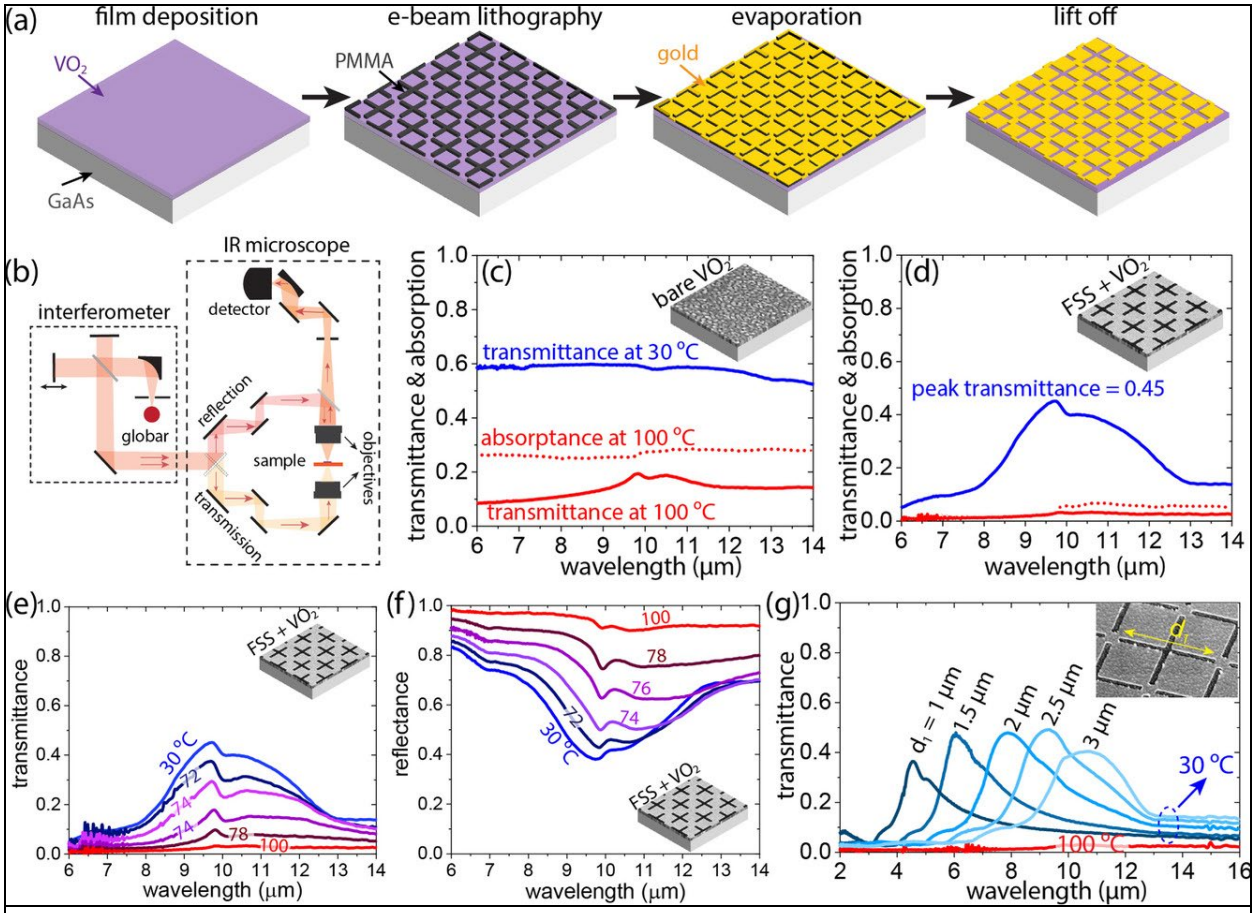

Figure 15. a) Fabrication flow for the reflective limiters based on VO_2 films (phase-transition material) and frequency-selective surfaces. The resulting structures are gold aperture antennas on top of a VO_2 film, on a transparent substrate. b) A schematic of simplified optical path of our transmission and reflection measurements, using an infrared microscope attached to a Fourier-transform spectrometer. c) Transmittance and absorptance spectra of the as-grown VO_2 film, for both insulating (30 °C) and metallic (100 °C) phases. d) Transmittance and absorptance spectra of the FSS-VO_2 limiter at 30 °C (open state) and 100 °C (limiting state). e,f) Transmittance and reflectance measurements of our fabricated FSS-VO_2 limiter when VO2 in its pure insulating phase (30 °C), pure metallic phase (100 °C), and intermediate phases across the IMT (at 72, 74, 76, and 78 °C). g) Measured transmittance of the FSS-VO_2 limiters with aperture lengths d_1 of 1, 1.5, 2, 2.5, and 3 μm, for both open (30 °C) and limiting (100 °C) states. The top surfaces of the inset figures in (c–g) are SEM images of the corresponding fabricated samples. Reproduced from C. Wan et al, *Laser & Photonics* News 15, 2100001 (2021).

The experimental demonstration of our optical limiter operating as a limiter can be found in Fig. 16, which shows limiting behavior using a laser. The limiting behavior is much stronger and occurs at a lower temperature (farther way from the VO_2 transition point) compared to a reference VO_2 film.

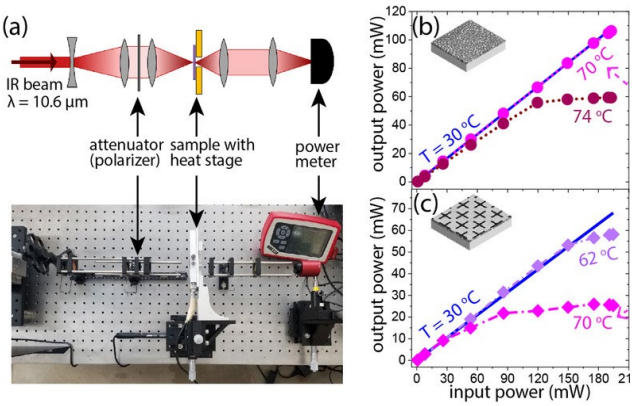

Figure 16. a) Our optical-limiter measurement setup using a continuous-wave CO_2 laser (λ = 10.6 μm) as the light source and a heat stage for thermal biasing. b, c) Power-dependent transmission measurements of (b) the bare VO_2 film and (c) the FSS-VO_2 limiter when they thermally biased at different temperatures. Reproduced from C. Wan et al, *Laser & Photonics* News 15, 2100001 (2021).

This work was featured on the cover of *Laser & Photonics Reviews* (Fig. 17).

Figure 17. Cover of our *Laser & Photonics Reviews*, featuring our recent publication on reflective optical limiters Reproduced from C. Wan et al, *Laser & Photonics* News 15, 2100001 (2021).

Optical forces and light sails

Following discussion with PO Gernot Pomrenke, we have also used this project to explore the science and engineering of optical forces on structured materials, in particular for applications in laser propulsion. Significant interest has built up over the last several years for "laser light sails", which are the laser-driven equivalent of solar sails. Together with the groups of Victor Brar (UW-Madison Physics) and Min Jang (KAIST), we computationally explored designs to make stable sails: that is, laser sails that self-correct their position and orientation if they begin to shift out or turn away from the incident laser beam. This problem is less acute for solar sails since sunlight is not limited to a particular area, but is very acute for laser-light sails.

Our design, recently published as J. Siegel et al, *ACS Photonics* 6, 8, 2032 (2019), is shown schematically in Fig. 18. The design approach is to use dielectric metasurfaces that vary across the sail area, such that light incident on the left side of the sail is reflected toward the right, and light incident on the right part of the sail is incident toward the left, with some special considerations having to do with the reflected wavefronts and the magnitudes of the reflections form each region. Our final design, that we modeled theoretically and also computationally based on Si metasurfaces on SiO_2 substrates at a wavelength of 1.55 um where both material shave very low losses, is referred to as a "inverse cat-eye" (ICE) sail.

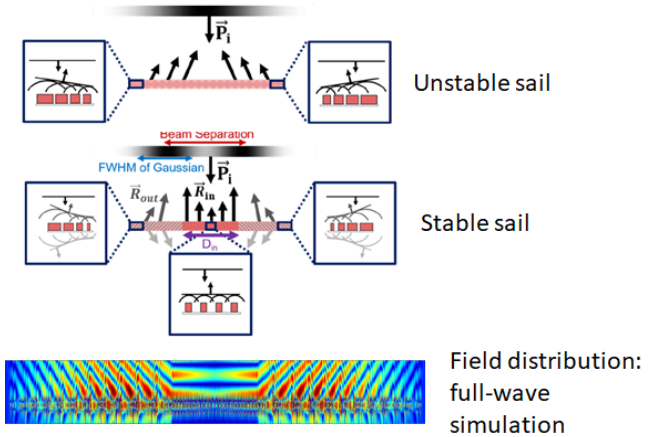

Figure 18. Schematic of our approach to stabilizing laser-light sails. By correctly engineering the magnitude and direction of the reflected beams across the sail, the sail can be stabilized against displacement and rotation, this maintaining its appropriate orientation in the beam. Reproduced from J. Siegel et al, *ACS Photonics* 6, 8, 2032 (2019).

We performed dynamical analysis on the displacement of the sail, δ, and the rotation of the sail θ as a function of time, taking parameters of the driving laser from those being explored for the Breakthrough Starshot initiative (Fig 19). We found that given appropriate design parameters, the ICE sail remains "stable" indefinitely and is able to ride the laser beam as it accelerates. Please note that "stable" here is in quotes, because the sail continues to oscillate as it rides the beam. Additional work is needed to understand how to parametrically cool the sail such that it not only continues to ride the beam but also is truly stable with the oscillation amplitude going to zero. Please also note that we explored both two-dimensional and three-dimensional sails from a

dynamical perspective, but we were only able to simulate the 2D case using full-wave simulations due to the enormous size of the 3D simulations that were ultimately intractable. We anticipate that making and measuring the forces on the sail may be a better future approach than full 3D simulations of the sail.

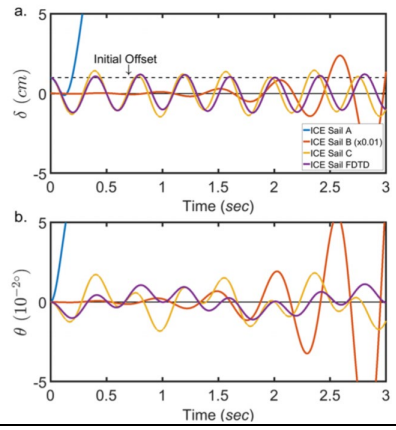

Figure 19. Plots of the displacement (a) and rotation (b) for three different sail and beam combinations over a three second time interval. The parameters for sail size and driving laser beam are taken from the goals of the Breakthrough Starshot initiatives.

Calculation and interpretation of optical forces

The exploration of optical forces for laser-driven propulsion of objects in space has recently become a field of significant interest for the community, driven in part by a recent privately funded effort from the Breakthrough Institute to develop laser sails for propulsion of small craft to Proxima Centauri (disclosure: I am a co-PI, together with Brar and Jang, on a project from the Breakthrough Institute, that was made possible by preliminary work funded on this project). As a result, it has become even more important than before to be able to calculate optical forces from optical field distributions, since the latter can be reliably simulated using various computational techniques such as the finite-difference time-domain (FDTD) method or the finite-element method (FEM).

There have been long-standing debates over how to calculate optical forces from fields. For example, standard textbooks teach that optical forces can be calculated from electromagnetic fields using the Lorentz force law, however other formalisms that are somewhat different exist as well. About a decade ago, Masud Mansuripur (Arizona) began arguing that in certain situations the Lorentz force law gives incorrect results, and that the appropriate formalism to use is the mostly forgotten Einstein-Laub formalism. Debates are still ongoing in the literature about the relative merits of these and other formalisms, and the issue is not settled. To me, the issue is related to the Abraham-Minkowski dilemma, which has to do with how to appropriately assign momentum to light vs to the polarized medium, when light is propagating through a medium.

However, even beyond the debates about force formalisms, there are other issues as well. As I discussed in the previous reports, our group has been looking at a set of papers from Kevin Webb at Purdue University that showed surprising results: that a nanostructured metal surface can be accelerated faster than a flat mirror would be given the same amount of incident light. Specifically, we were looking at the result of Velzen and Webb, Phys. Rev. B 92, 115416 (2015), but there are several other papers following up on this paper with similar conclusions.

One structure that Velzen and Webb explored is schematically shown in Fig. 20: a gold film with periodic slits, and light incident from above the structure from free space. The surprising result of this paper is that the optical forces on a metallic structure such as the periodic structure in Fig. 1 can be much larger than the optical forces on a flat metal mirror (i.e., the same metal structure but with no corrugation). This result appears to be at odds with conservation of momentum, and thus reconciling it with well-established principles relating to the conservation of momentum and the momentum of light in free space will be important: either it will mean a breakdown of very well established physics (much less likely, in our view) or it will give us an understanding of issues with these type of force calculations (much more likely in our view).

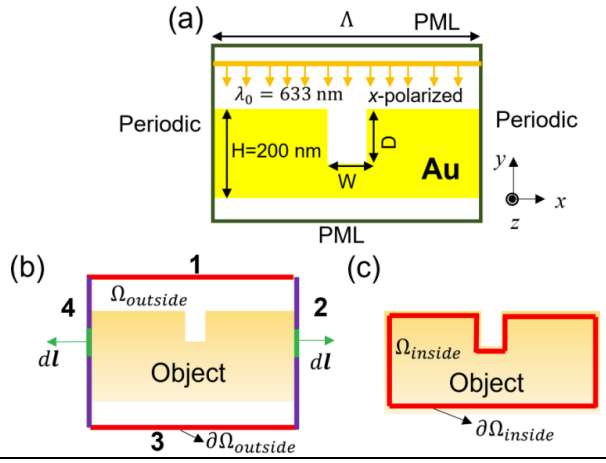

Figure 20. (a) An Au film in free space with periodic slits on the top surface illuminated from the top. (b) and (c) Two choices of the force calculation region Ω for the periodic structure. (b) Outside choice: $\partial\Omega$ consists of two segments in free space and two segments that overlap the periodic boundaries. (c) Inside choice: $\partial\Omega$ is are within the homogeneous object but as close as possible to the boundaries of the object. From our Feng et al, *Physical Review B* 105, 207401 (2022).

After performing our own extensive calculations, we have submitted a Comment to Physical Review B to summarize our findings, which has now been published as Feng et al, *Physical Review B* 105, 207401 (2022). This comment includes our own re-calculation of electromagnetic in the structure (which match those of Velzen and Webb) and force densities using both the Einstein-Laub formalism (which was used by Velzen and Webb) and the Lorentz formalism. We have taken

great care to make sure the calculations are correct, including a significant amount of convergence testing and cross checking. For this structure, all of the field and force-density calculations that we performed are consistent with those of Velzen and Webb. However, the *total forces* we calculated were different from the result of Velzen and Webb, and are not in conflict with any radiation-pressure bounds resulting from the well-established physical concepts of momentum conservation and the momentum of light in free space (Fig. 21).

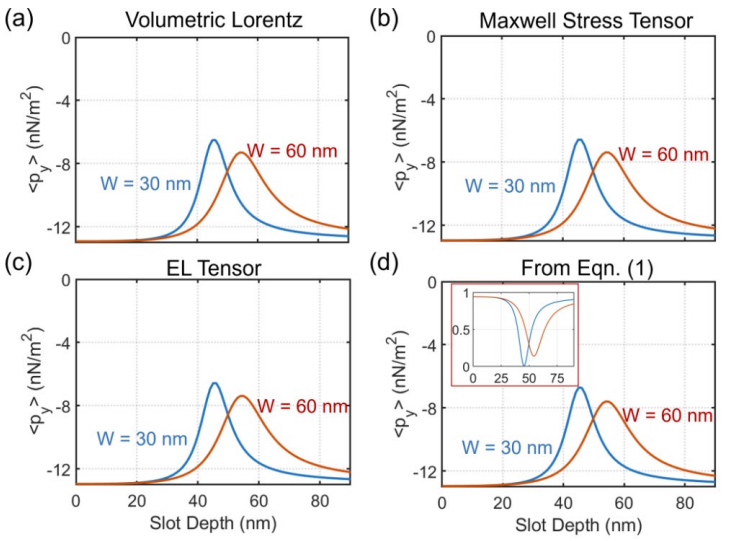

Figure 21. Calculated time-averaged optical pressure as a function of slot depth based on (a) the volumetric Lorentz method, (b) the Maxwell Stress Tensor (MST) method, (c) the Einstein-Laub (EL) tensor method, and (d) a simple radiation-pressure calculation based on the simulated reflectance. In all cases, $\Omega = \Omega_{outside}$. The minus sign means that the direction of the optical force is in the −y direction. The far-field reflectance as a function of slot depth is shown as an inset. From our Feng et al, *Physical Review B* 105, 207401 (2022).

Our understanding is that the difference between our results and those of Velzen and Webb lies in the integration boundaries, when integrating the optical forces. This difference can be seen in Fig. 1: in one case, the integration bound is on the outside of the object (segments 2 and 4 in Fig. 1(b) do not actually count here because they are along periodic boundary conditions, and therefore all contributions along those segments cancel out), and in the other case the integration bound is on the inside of the object, just inside the physical boundary. Though conceptually these two integration bounds should give the same result, they apparently do not because there is a delta-function-like force contribution right at the boundary in both the Lorentz and Einstein-Laub formalisms. This can be seen in Fig. 22 below, showing the large differences between the different choice of integration boundary as a function of simulation mesh size. Better understanding of this (likely nonphysical) delta-function-like force contribution at the interface will help us find a way to accurately treat force densities and forces due to electromagnetic fields.

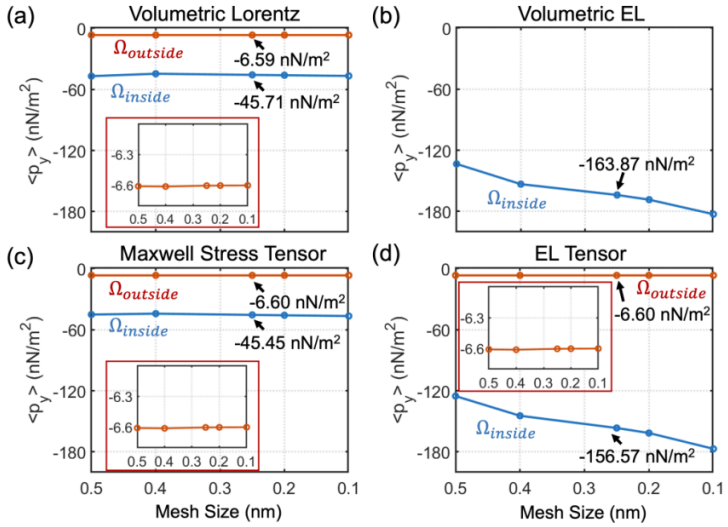

Figure 22. Total time-averaged optical pressure on the structure in Fig. 1 (with W = 30 nm and D = 46 nm), calculated using (a) the volumetric Lorentz method, (b) the volumetric EL method, (c) the MST method, and (d) the EL tensor method with both $\Omega_{outside}$ and Ω_{inside} applied as a function of simulation mesh size. For panels (a), (c), and (d), we show the zoomed-in plots of the results using $\Omega_{outside}$ to demonstrate convergence. From our Feng et al, *Physical Review B* 105, 207401 (2022).

Please note this is a purely scientific disagreement. Our viewpoint is that such debates -- done in a careful and respectful fashion, including the appropriate peer-review channels in established journals -- are helpful to the scientific enterprise and should be encouraged.